Chaos
An Interdisciplinary Journal of Nonlinear Science

RESEARCH ARTICLE | OCTOBER 21 2024

On coupled oscillators modeling bio-inspired acoustic sensors: Bifurcation analysis toward tunability enhancement

H. F. J. Rolf ; T. Meurer

Chaos 34, 103135 (2024)
https://doi.org/10.1063/5.0217847

On coupled oscillators modeling bio-inspired acoustic sensors: Bifurcation analysis toward tunability enhancement

Cite as: Chaos 34, 103135 (2024); doi: 10.1063/5.0217847
Submitted: 7 May 2024 · Accepted: 3 October 2024 ·
Published Online: 21 October 2024

View Online Export Citation CrossMark

H. F. J. Rolf[a),b)] and T. Meurer[b)]

AFFILIATIONS

Digital Process Engineering Group, Institute of Mechanical Process Engineering and Mechanics, Karlsruhe Institute of Technology, Hertzstr. 16, D-76187 Karlsruhe, Germany

[a)]**Author to whom correspondence should be addressed:** folke.rolf@kit.edu
[b)]**URL:** https://www.mvm.kit.edu/english/dpe.php

ABSTRACT

Oscillators exhibiting an Andronov–Hopf bifurcation are candidates to mimic the functionality of the cochlea, since the transfer response of these oscillators is compressive and frequency selective. The former implies that small stimuli are amplified and strong stimuli are attenuated, while the latter means that the oscillator only reacts in a (small) frequency band. However, this implies that many oscillators are needed to cover a relevant frequency band. By introducing the notion of tunable characteristic frequencies, i.e., the characteristic frequency can be adjusted by a controllable input, the number of oscillators can be eventually reduced. Subsequently, the tunability enhancement of coupled oscillators is investigated by analyzing the local dynamics of a network of oscillators. For this, necessary conditions for the emergence of Andronov–Hopf bifurcations are determined for networks consisting of two groups, i.e., a group is a network of identical oscillators. By choosing the eigenvalues of the product of the cross-coupling matrix as bifurcation parameters and exploiting the structure of the transfer matrix of this network, the critical points and, thus, the characteristic frequency at this point can be derived. Tunability of the characteristic frequency is then enabled by controlling the asymmetry between the groups of oscillators.

In rapidly changing environments, technological speech procession is outperformed by mammalian hearing perception. This comes from the fact that hearing perception is superior in terms of energy and time consumption, which is induced by a nonlinear feedback loop in the cochlea. In particular, the dynamics of the feedback loop is similar to an Andronov–Hopf bifurcation. Thus, oscillators exhibiting this bifurcation can mimic the functionality of the cochlea so that the performance gap might be closed by implementing them into technology. However, many oscillators are needed since a system exhibiting an Andronov–Hopf bifurcation can only react to a (small) frequency range. Hence, methods to reduce this number are needed. This can be done, e.g., by enabling tunability of the characteristic frequency so that one oscillator can measure a frequency band. In this work, the influence of coupling oscillators on the dynamics is analyzed. In particular, it is shown that by coupling, the Andronov–Hopf bifurcation is preserved and the characteristic frequency becomes tunable.

I. INTRODUCTION

Compared to technical solutions, the auditory perception of mammalians is superior. This performance difference comes from the different architectures of both systems: the technical solution has a feedforward structure consisting of three steps—a typical micro-electromechanical microphone with a passive, linear characteristics,[1] nonlinear pre-processing,[2] and an artificial neural network[3,4]—while auditory perception has a feedback structure that induces an active process with a compressive nonlinearity.[5,6] The latter implies that the dynamical range of the biological system is significantly extended compared to a feedforward architecture.

Furthermore, auditory perception is frequency selective. With this, the biological system can detect both faint sound with low background noise and sound, which is heavily jammed, i.e., the latter effect is called the cocktail party effect.[7,8] This high adaptability is also induced by the feedback loop, which is summarized subsequently.

The nonlinear dynamics of the auditory perception are located in the cochlea, where the pressure of an acoustic signal is transformed into an electrical signal. This is done by the interplay of the basilar membrane, the tectorial membrane, and the inner and outer hair cells. The inner hair cells are only connected to the basilar membrane, so these are hyperpolarized by bending them to one direction and are depolarized by bending them to the opposite direction. In contrast, the outer hair cells are connected both to the basilar membrane and the tectorial membrane and the stiffness of these hair cells can be changed. Thus, they can either block the inner hair cells from oscillating or amplify a signal by stimulating the inner hair cells by using the tectorial membrane. Moreover, the basilar membrane is frequency selective, so higher frequencies stimulate the front of the basilar membrane and lower frequencies stimulate its end.[11,12] Note that the feedback mechanism of the inner and the outer hair cells couples to their neighbors since they are connected by the tectorial membrane. Hence, the cochlea can be viewed as oscillators coupled in a line topology.

Modeling of the cochlea commonly involves the ability to generate an Andronov–Hopf bifurcation as moving from the sub-critical to the super-critical regime (and vice versa) induces useful dynamical properties to mimic biological behavior. In the sub-critical regime, a system exhibiting an Andronov–Hopf bifurcation is asymptotically stable. After exceeding the critical point, the system can exhibit a stable limit cycle. Thus, by proving that this type of bifurcation exists, the existence of a limit cycle can be concluded.[13] In addition, the synchronization problem can be addressed for coupled oscillators.[14] Hence, the emergence of Andronov–Hopf bifurcations was analyzed for various systems arising, e.g., in engineering,[15] biology,[16–19] and physics.[14,20,21] Moreover, systems exhibiting Andronov–Hopf bifurcations have remarkable properties in the sub-critical regime. Here, the response to an excitation can be either linear if the system is far away from the critical point or both frequency selective and compressive, if the system is close to the critical point. Thus, a system exhibiting an Andronov–Hopf bifurcation has similar dynamical properties as the cochlea.[22–24] This implies in view of the realization of a bio-inspired sensor mimicking the functionality of the cochlea that Andronov–Hopf bifurcations must be enabled by design and/or suitable feedback control so that both the linear and the nonlinear properties in the sub-critical regime can be used to enhance sensor performance. Additionally, coupling these sensors may enhance frequency tunability[20,25] or may enable broader bandwidth[26] of the response in terms of external input. Thus, improving the performance of the system.

It was shown in Lenk *et al.*[9] that this behavior can be realized in principle utilizing a thermally actuated, micro-electromechanical cantilevered (MEMS) sensor. Mathematically, this system can be modeled as a linear Euler–Bernoulli beam with a nonlinear actuation induced by the embedded heater. The deflection can be measured with an embedded piezoelectric sensor[27] so that the velocity can be computed using a high pass filter. By considering a dominant mode approximation and by feeding back the velocity with a suitable gain, two different Andronov–Hopf bifurcations can be achieved as was shown experimentally in Refs. 9, 26, 28, and 29 and theoretically in Refs. 9 and 10. The principle bifurcation behavior is sketched in Fig. 1. Particularly, the system is locally asymptotically stable in the interval $[k_{H,2}, k_{H,2}]$. After surpassing the critical value $k_{H,1}$ or by falling below the critical value $k_{H,2}$, an unstable limit cycle will emerge in the dominant mode model.[10] In view of the conceptually similar dynamics, this device can also be called an artificial hair cell. However, different issues remain as for a single sensor the characteristic frequency of the model cannot be adjusted simultaneously in this way. Ideally, this can be changed by exploiting a controllable asymmetry of coupled MEMS sensors, such that the characteristic frequencies of the network can be changed by assigning the damping accordingly. For instance, a change in the characteristic frequency can be observed with two injectively coupled Andronov–Hopf oscillators in Gomez *et al.*[20] and Rolf and Meurer.[25]

In contrast, symmetry and symmetry-breaking is commonly investigated. Herein, the oscillators are assumed to be symmetric for some group, e.g., identical oscillator coupled in an undirected graph, such that the symmetry-breaking of equivariant ordinary differential equations (ODEs) can be shown by applying the equivariant branching lemma for the analysis of steady state bifurcations, e.g., saddle-node bifurcations, and the equivariant Hopf theorem for the analysis of the Andronov–Hopf bifurcation in these networks.[30] In particular, multi-clustering and pattern formation appear after the symmetry breaks. Thus, symmetry and symmetry-breaking can be used to describe, for instance, animal gaits and central pattern generators[31–33] and specification.[34–37]

A different approach to simplify the analysis of coupled oscillators is the assumption that the coupling is weak. Then, each oscillator in the network can be described as an uncoupled oscillator with a small perturbation resembling the coupling between the oscillators. With this assumption, the models of the oscillators can be simplified to a phase model by applying perturbation methods.[38] Note that different methods are needed to compute the phase models since the dynamics of the oscillators can be, for example, stiff or non-stiff.[39–41] For instance, this simplification can be used to investigate chemical reactions[42,43] and neuronal networks.[44]

This paper aims to analyze the tunability enhancements of asymmetric coupled oscillators. This is done by analyzing the bifurcation behavior of two coupled groups of MEMS sensors with a focus on the emergence of Andronov–Hopf bifurcations and the qualitative behavior of the corresponding characteristic frequencies. Herein, the bifurcation parameters are assumed to be the eigenvalues of the product between the cross-coupling matrix and the internal feedback of the MEMS sensors is used to induce a controllable asymmetry in the network. It should be noted that the bifurcation analysis extends the results in Stan and Sepulchre,[15] where the coupling of identical oscillators in symmetric networks is addressed. In particular, the necessary condition is shown by transforming the transfer function of the uncoupled system with the adjacency matrix into a weighted identity matrix. A rank drop satisfying the necessary condition of the Andronov–Hopf bifurcation can be easily shown for the network consisting of two groups of oscillators. The characteristic frequencies then follow from the

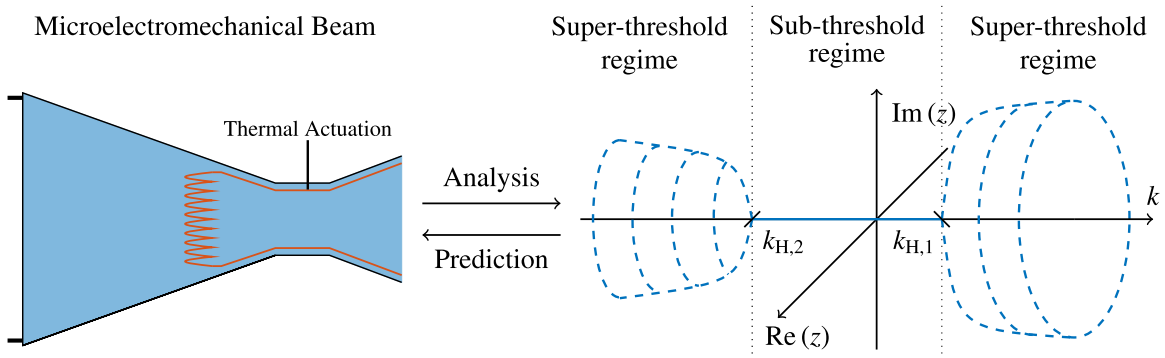

FIG. 1. The properties of a MEMS sensor resembling an artificial hair cell are predicted by mathematical analysis. (Left) Sketch of MEMS sensor resembling an artificial hair cell. The experimental setup consisting of the MEMS sensor and an FPGA has been designed by Kalpan Ved, Vishal Gubbi, Tzvetan Ivanov, Claudia Lenk, and Martin Ziegler (all from TU Ilmenau). (Right) Sketch of the bifurcation diagram of an artificial hair cell. Herein, z and k are the state of the center manifold of the Andronov–Hopf bifurcation and the bifurcation parameter of the system. Moreover, the two bifurcation points are denoted by $k_{H,1}$ and $k_{H,2}$. Herein, the locally asymptotically stable regime is depicted by a solid line and the unstable regime is depicted by a dashed line, respectively.[9,10]

bifurcation analysis and conditions for the tunability of the characteristic frequency as a function of the internal feedback are derived. In addition, the location of the critical points is analyzed by determining the critical point of a so-called Hopf–Hopf bifurcation.[30,45,46] With this, the characteristic frequency in the sub-critical regime is characterized.

The paper is structured as follows: In Sec. II, the dominant mode model of a coupled MEMS sensor is introduced and the preliminaries for the local analysis and the challenges in analyzing the bifurcations are discussed. Afterward, the notion of tunability is defined in Sec. III. In addition, it is shown that a single MEMS sensor is not tunable to motivate the bifurcation analysis for a network of MEMS sensors. Then, two groups of identical and non-identical MEMS sensors are analyzed in Sec. IV with respect to the emergence of Andronov–Hopf bifurcations. Herein, the controllable asymmetry between two groups of non-identical is used to achieve tunability of the system. The results are then numerically verified in Sec. V. The focus of the simulation studies is to provide insight if the Andronov–Hopf bifurcation of the coupled, MEMS sensors is tunable and to compare the reaction of the bio-inspired system with the cochlea. Finally, some remarks conclude this paper.

II. NETWORKS OF MEMS SENSORS

Subsequently, the dominant mode model of the MEMS sensor is introduced. For instance, a picture of a MEMS sensor is illustrated on the left side of Fig. 1 and in Fig. 2. The model is derived from a distributed parameter model of a thermally actuated micro-mechanical Euler–Bernoulli beam with embedded thermal actuation.[27,47] In this sense, the mathematical model of the ith MEMS sensor in a network of $N \in \mathbb{N}$ MEMS sensors is described by

$$\dot{\boldsymbol{x}}_i = \boldsymbol{f}_i(\boldsymbol{x}_i), \qquad t > 0, \qquad \boldsymbol{x}_i(0) = \boldsymbol{x}_{0,i}, \tag{1a}$$

$$y_i = \boldsymbol{h}(\boldsymbol{x}_i) = x_{i,4}, \qquad t \geq 0, \tag{1b}$$

with the vector-valued nonlinearity,

$$\boldsymbol{f}_i(\boldsymbol{x}_i) = \begin{bmatrix} x_{i,2} \\ -\omega_i^2 x_{i,1} - \frac{\omega_i}{Q_i} x_{i,2} + \alpha_i x_{i,3} + \frac{p}{\rho h} \\ -\beta_i x_{i,3} + \zeta_i u_{\mathrm{act},i}^2 \\ -\frac{1}{\tau_i} x_{i,4} + \kappa_i x_{i,2} \end{bmatrix}. \tag{1c}$$

The state vector, the output, the controllable voltage, the sound pressure, and the initial condition are denoted by $\boldsymbol{x}_i(t) \in \mathbb{R}^4$, $y_i(t) \in \mathbb{R}$, $u_{\mathrm{act},i}(t) \in \mathbb{R}$, $p(t) \in \mathbb{R}$, and $\boldsymbol{x}_{0,i} \in \mathbb{R}^4$ for the oscillators $i = 1, 2, \ldots, N$. Herein, the state vector $\boldsymbol{x}_i$ consists out of the deflection $x_{i,1}(t) \in \mathbb{R}$, the velocity $x_{i,2}(t) \in \mathbb{R}$, the temperature relative to the room temperature $x_{i,3}(t) \in \mathbb{R}$, and the voltage of a high pass filter $x_{i,4}(t) \in \mathbb{R}$. Additional parameters are the heater constant $\zeta_i = \gamma_i / R_i^2$, the natural frequency $\omega_i > 0$, the Q-factor $Q_i > 0$, the transfer factors $\alpha_i, \gamma_i > 0$, the time constants $\beta_i, \tau_i > 0$, the calibration factor $\kappa_i \in \mathbb{R}$, the heater resistance $R_i > 0$, the height $h > 0$, and the density $\rho > 0$. In particular, the high pass filter in terms of the state $x_{i,4}$ is used to remove a constant signal offset so that the amplification is independent to the pre-deflection of the cantilever. A sketch of the network is shown in Fig. 2.

The main goal of this paper is to investigate the dynamics of a network of MEMS sensors. Herein, a network structure is imposed by using output feedback,

$$u_{\mathrm{act},i} = g_i(\boldsymbol{\chi}_4) + \nu_i = \sum_{j=1}^{N} k_{ij} x_{j,4} + \nu_i, \quad \forall i = 1, 2, \ldots, N, \tag{2}$$

with the outputs of each oscillator summarized in the vector $\boldsymbol{\chi}_4 = [x_{1,4}, \ldots, x_{N,4}]^{\mathrm{T}} \in \mathbb{R}^N$, additional inputs $\nu_i(t) \in \mathbb{R}$, and k_{ij} referring to the entries of the adjacency matrix of the network $K \in \mathbb{R}^{N \times N}$. To identify the dynamics of this network, the local bifurcations are analyzed. For this, the feedback and the coupling have to influence the linearization of the coupled, MEMS sensors in a dedicated way, such that an Andronov–Hopf bifurcation can emerge.[13,45] In particular, the eigenvalues of the adjacency matrix K are of interest for the

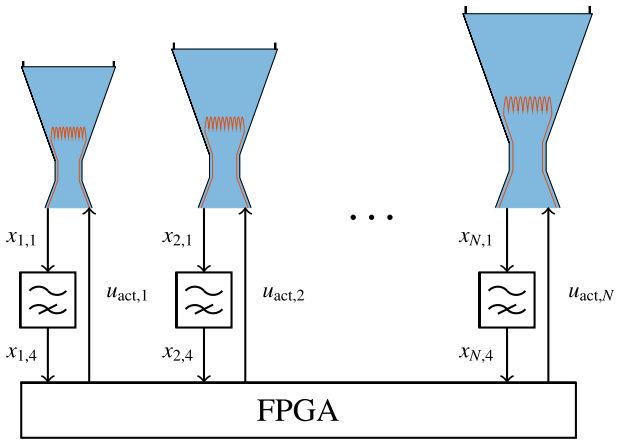

FIG. 2. Sketch of a network of coupled, MEMS sensors. The coupling of the MEMS sensors is processed inside the FPGA. Herein, the different sizes of the MEMS sensors depict different natural frequencies. For practical interpretation, a larger MEMS sensor usually has a smaller natural frequency. The experimental setup consisting of the MEMS sensor and an FPGA has been designed by Kalpan Ved, Vishal Gubbi, Tzvetan Ivanov, Claudia Lenk, and Martin Ziegler (all from TU Ilmenau).

bifurcation analysis and to compute the characteristic frequency as is elaborated in Secs. IV and V.

To determine the necessary condition for the emergence of an Andronov–Hopf bifurcation, i.e., a pair of complex conjugated eigenvalues on the imaginary axis, the equilibria of (1) have to be determined. This is done by solving $\boldsymbol{f}_i(\boldsymbol{\chi}_{\mathrm{eq}}) = 0$ for constant input $u_{\mathrm{DC},i} = v_{\mathrm{eq},i} \in \mathbb{R}$. As expected, the high pass removes the DC components from the feedback (2) so that the equilibrium of the network is given by the composition of the equilibrium of each individual MEMS sensor, i.e.,

$$\boldsymbol{x}_{i,\mathrm{eq}} = \begin{bmatrix} \frac{\alpha_i \zeta_i}{\beta_i \omega_i^2} u_{\mathrm{DC},i}^2 & 0 & \frac{\zeta_i}{\beta_i} u_{\mathrm{DC},i}^2 & 0 \end{bmatrix}^{\mathrm{T}}. \tag{3}$$

In particular, (3) implies that the DC-component of the actuation voltage directly influences the equilibrium values of the deflection $x_{i,\mathrm{eq},1}$ and the relative temperature $x_{i,\mathrm{eq},3}$. In addition, the coupling and the feedback appear in the linearization, if $u_{\mathrm{DC},i} \neq 0$. The DC-component $u_{\mathrm{DC},i}$ is, hence, necessary to control the local dynamics of (1). For simplicity, let the state and input vector of the network be $\boldsymbol{\chi}(t) = [\boldsymbol{x}_1^{\mathrm{T}}(t), \boldsymbol{x}_2^{\mathrm{T}}(t), \ldots, \boldsymbol{x}_N^{\mathrm{T}}(t)]^{\mathrm{T}} \in \mathbb{R}^{4N}$ and $\Delta\boldsymbol{v}(t) = [\Delta v_1(t), \Delta v_2(t), \ldots, \Delta v_N(t)]^{\mathrm{T}} \in \mathbb{R}^N$. Then, the linearization is given by

$$\Delta\dot{\boldsymbol{\chi}} = A\Delta\boldsymbol{\chi} + B\begin{bmatrix} p\mathbb{1}_N \\ \Delta\boldsymbol{v} \end{bmatrix},$$

$$\boldsymbol{y} = C\Delta\boldsymbol{\chi},$$

with $\Delta\boldsymbol{\chi} = \boldsymbol{\chi} - \boldsymbol{\chi}_{\mathrm{eq}}$, $\Delta\boldsymbol{v} = \boldsymbol{v} - \boldsymbol{u}_{\mathrm{DC}}$, the vector of ones $\mathbb{1}_N \in \mathbb{R}^N$, and the matrices

$$A = \left.\frac{\partial \boldsymbol{f}}{\partial \boldsymbol{\chi}}\right|_{\boldsymbol{\chi}=\boldsymbol{\chi}_{\mathrm{eq}}, \boldsymbol{v}=\boldsymbol{u}_{\mathrm{DC}}} = [A_{ij}]_{i,j=1,\ldots,N} \in \mathbb{R}^{4N\times 4N},$$

$$B = \left.\frac{\partial \boldsymbol{f}}{\partial \boldsymbol{v}}\right|_{\boldsymbol{\chi}=\boldsymbol{\chi}_{\mathrm{eq}}, \boldsymbol{v}=\boldsymbol{u}_{\mathrm{DC}}} = [B_{ij}]_{i,j=1,\ldots,N} \in \mathbb{R}^{4N\times 2N},$$

$$C = \left.\frac{\partial \boldsymbol{h}}{\partial \boldsymbol{\chi}}\right|_{\boldsymbol{\chi}=\boldsymbol{\chi}_{\mathrm{eq}}, \boldsymbol{v}=\boldsymbol{u}_{\mathrm{DC}}} = [C_{ij}]_{i,j=1,\ldots,N} \in \mathbb{R}^{N\times 4N},$$

where the sub-matrices A_{ij}, B_{ij}, and C_{ij} are given by

$$A_{ii} = \begin{bmatrix} 0 & 0 & 1 & 0 \\ -\omega_i^2 & -\frac{\omega_i}{Q_i} & \alpha_i & 0 \\ 0 & 0 & -\beta_i & \varepsilon_i k_{ii} \\ 0 & \kappa_i & 0 & -\frac{1}{\tau} \end{bmatrix}, \quad A_{ij} = \begin{bmatrix} 0 & 0 & 0 & 0 \\ 0 & 0 & 0 & 0 \\ 0 & 0 & 0 & \varepsilon_i k_{ij} \\ 0 & 0 & 0 & 0 \end{bmatrix},$$

$$B_{ii} = \begin{bmatrix} 0 & \frac{1}{h\rho} & 0 & 0 \\ 0 & 0 & \varepsilon_i & 0 \end{bmatrix}^{\mathrm{T}}, \quad B_{ij} = 0,$$

$$C_{ii} = \begin{bmatrix} 0 & 0 & 0 & 1 \end{bmatrix}, \quad C_{ij} = 0,$$

with the coefficient $\varepsilon_i = 2\zeta_i u_{\mathrm{DC},i}$. Particularly, the diagonal blocks of the system matrix A consist of the (linearized) system dynamics of the individual MEMS sensors and the off-diagonal blocks of the system matrix A describe the coupling between the MEMS sensors. In addition, the characteristic polynomial of the system matrix is of degree $4N$. Thus, this polynomial is, in general, not analytically solvable[48,49] so that the necessary conditions of an Andronov–Hopf bifurcation cannot be investigated directly. To circumvent this issue, the structure of the system matrix A is exploited subsequently by considering the transfer function of an uncoupled MEMS sensor,

$$\begin{aligned} g_i(s) &= C_{ii}\left(sI - A_{ii}\right)^{-1} B_{ii} \\ &= \frac{b_{i1}s}{s^4 + a_{i3}s^3 + a_{i2}s^2 + a_{i1}s + a_{i0}}, \end{aligned} \tag{4}$$

where the coefficients are given by

$$a_{i0} = \frac{\beta_i \omega_i^2}{\tau_i}, \tag{5a}$$

$$a_{i1} = \beta_i \omega_i^2 + \frac{\beta_i \omega_i}{Q_i \tau_i} + \frac{\omega_i^2}{\tau_i}, \tag{5b}$$

$$a_{i2} = \frac{\beta_i}{\tau_i} + \frac{\beta_i \omega_i}{Q_i} + \frac{\omega_i}{Q_i \tau_i} + \omega_i^2, \tag{5c}$$

$$a_{i3} = \beta_i + \frac{\omega_i}{Q_i} + \frac{1}{\tau_i}, \tag{5d}$$

$$b_{i1} = 2\alpha_i \kappa_i \zeta_i u_{\mathrm{DC},i} \tag{5e}$$

for the oscillator $i = 1, 2, \ldots, N$. Obviously, the degree of the denominator polynomial of $g_i(s)$ is in general identical to the system order. Hence, no cancellation between zeros and poles occurs.

III. PROBLEM STATEMENT

In addition to determining the dynamics of the coupled MEMS sensors, the number of oscillators in an acoustic sensor has to be reduced and the design has to be robust. This can be done, e.g., by asserting that the characteristic frequency is adjustable by external

feedback. This property of an oscillator or a network of oscillators is subsequently called (frequency) tunability.

Definition 1 (Frequency tunability). *An oscillator or a network of oscillators is called tunable, if its characteristic frequency (or synchronization frequency, respectively) can be changed by a controllable input. In addition, the parameter controlling the (frequency) tunability of the oscillator or network of oscillators is called tunability parameter.*

It should be noted that Definition 1 is not satisfied in general for an oscillator and that this property can be induced in a MEMS sensor by changing the geometry of the MEMS sensor,[47,50–56] so that geometric nonlinearities arise for small pre-deflections of the MEMS sensor. For instance, these nonlinearities can then be modeled by a Duffing oscillator.[47] In contrast to this, subsequently frequency tunability is investigated by exploiting asymmetries between coupled oscillators so that the frequency can be tuned without adapting the geometry of the MEMS sensor.

A. Example 1: Tunability of two coupled Kuramoto oscillators

To visualize that coupling can induce frequency tunability, the characteristic frequency of two coupled Kuramoto oscillators as a function of the coupling strength is discussed. Kuramoto oscillators are coupled phase models of an oscillator with constant frequency. Two coupled Kuramoto oscillators are, e.g., governed by[57]

$$\dot{\varphi}_1 = \omega_1 + \gamma_{12}\sin(\varphi_2 - \varphi_1), \qquad t > 0, \varphi_1(0) = \varphi_{1,0}, \tag{6a}$$

$$\dot{\varphi}_2 = \omega_2 + \gamma_{21}\sin(\varphi_1 - \varphi_2), \qquad t > 0, \varphi_2(0) = \varphi_{2,0}, \tag{6b}$$

with the phases $\varphi_1(t), \varphi_2(t) \in \mathbb{R}$ and the initial conditions $\varphi_{1,0}$, $\varphi_{2,0} \in \mathbb{R}$. The parameters are given by the frequencies $\omega_1, \omega_2 > 0$ and the coupling $\gamma_{12}, \gamma_{21} \in \mathbb{R}$. In addition, assume that the frequencies ω_1 and ω_2 are fixed, while the coupling γ_{12} and γ_{21} are assumed to be controllable and, hence, serve as the tunability parameters. Subsequently, the frequency tunability of system (6) is analyzed by comparing the dynamics of the synchronized system, i.e., $\dot{\varphi}_C = \omega_C(\gamma_{12}, \gamma_{21})$ with the characteristic frequency $\omega_C(\gamma_{12}, \gamma_{21}) > 0$. This can be done by computing the steady state of the phase error $\Delta\varphi_{12} = \varphi_1 - \varphi_2$. The dynamics of the phase error is given by

$$\Delta\dot{\varphi}_{12} = \omega_1 - \omega_2 - (\gamma_{12} + \gamma_{21})\sin(\Delta\varphi_{12}).$$

Asserting the steady state condition, i.e., $\Delta\dot{\varphi}_{12,\mathrm{eq}} = 0$, implies that the oscillators are synchronized and yields

$$\sin(\Delta\varphi_{12,\mathrm{eq}}) = \frac{\omega_1 - \omega_2}{\gamma_{12} + \gamma_{21}}. \tag{7}$$

In particular, (7) implies that two coupled Kuramoto oscillators can synchronize, if $|\omega_1 - \omega_2|/|\gamma_{12} + \gamma_{21}| \leq 1$. Inserting (7) into the dynamics (6) and comparing the result with the synchronized system results in the dynamics of the synchronized oscillators, whose characteristic frequency is given by

$$\omega_C(\gamma_{12}, \gamma_{21}) = \frac{\gamma_{21}\omega_1 + \gamma_{12}\omega_2}{\gamma_{12} + \gamma_{21}}.$$

Note that asymmetry of the coupling is necessary to enable tunability, since $\omega_C(\gamma, \gamma) = (\omega_1 + \omega_2)/2$ with the symmetric coupling $\gamma \in \mathbb{R}$. In addition, the characteristic frequency ω_C is closer to the frequency ω_i of the ith oscillator, if $\gamma_{ji} > \gamma_{ij}$ for all $i, j = 1, 2$ and $i \neq j$, and the characteristic frequency can be tuned in $[\omega_1, \omega_2]$, since $\gamma_{12} = 0$ implies $\omega_C = \omega_1$ and $\gamma_{21} = 0$ implies $\omega_C = \omega_2$. The characteristic frequency ω_C is visualized in Fig. 3. For this, the parameters are given by $\omega_1 = 40$ and $\omega_2 = 50$ and the relative coupling $\eta = \gamma_{12}/\gamma_{21}$ is introduced. The latter simplifies the characteristic frequency to

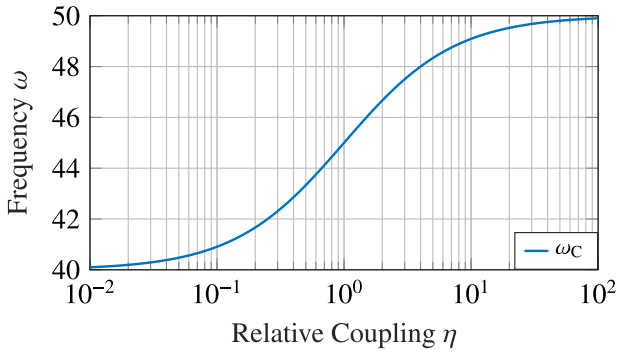

FIG. 3. Characteristic frequency ω_C of two coupled Kuramoto oscillators as a function of the relative $\eta = \gamma_{12}/\gamma_{21}$. The natural frequencies are given by $\omega_1 = 40$ and $\omega_2 = 50$.

$$\omega_C(\eta) = \frac{\omega_1 + \eta\omega_2}{\eta + 1}.$$

B. Example 2: Tunability of two injectively coupled Andronov–Hopf oscillators

As a second example, the characteristic frequency of two injectively coupled Andronov–Hopf oscillators is investigated. These oscillators are described by the super-critical normal form of the Andronov–Hopf bifurcation and the system is governed by

$$\dot{z}_1 = (\mu_1 + \mathrm{i}\omega_1)z_1 - |z_1|^2 z_1 + \gamma_{12}z_2, \qquad z_1(0) = z_{1,0}, \tag{8a}$$

$$\dot{z}_2 = (\mu_2 + \mathrm{i}\omega_2)z_2 - |z_2|^2 z_2 + \gamma_{21}z_1, \qquad z_2(0) = z_{2,0}, \tag{8b}$$

with the states $z_1(t), z_2(t) \in \mathbb{C}$, the damping parameters μ_1, $\mu_2 \in \mathbb{R}$, the natural frequencies $\omega_1, \omega_2 > 0$, and the coupling strengths $\gamma_{12}, \gamma_{21} \in \mathbb{R}$. Assume that the product of the coupling strengths is the bifurcation parameter. The critical point and the characteristic frequency of (8) are determined by[25]

$$\gamma_{12,\mathrm{H}}\gamma_{21,\mathrm{H}} = \frac{\mu_1\mu_2}{(\mu_1 + \mu_2)^2}\left[(\mu_1 + \mu_2)^2 + (\omega_1 - \omega_2)^2\right], \tag{9a}$$

$$\omega_C = \frac{\omega_1 + \omega_2}{2} - \frac{\mu_1 - \mu_2}{\mu_1 + \mu_2}\frac{\omega_1 - \omega_2}{2}. \tag{9b}$$

Similar to the previous example, the characteristic frequency at the critical point can be tuned by controlling the asymmetry between the damping μ_1 and μ_2 and the tunable interval is also restricted by the natural frequency of the oscillators. This is depicted in Fig. 4.

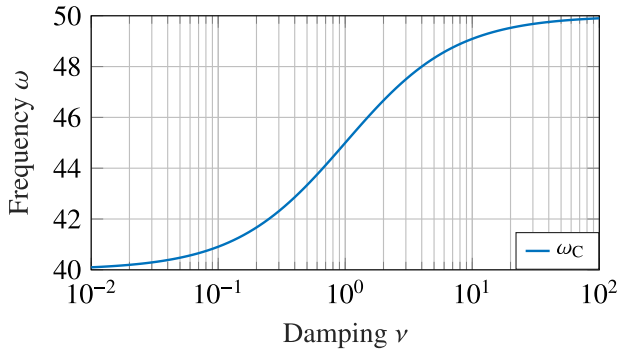

FIG. 4. Characteristic frequency ω_C of two injectively coupled Andronov–Hopf oscillators as a function of the relative $\nu = \mu_1/\mu_2$ with the natural frequencies $\omega_1 = 50$ and $\omega_2 = 60$.

For this, $\omega_1 = 50$ and $\omega_2 = 60$ are assigned and the relative damping $\nu = \mu_1/\mu_2$ is introduced to simplify the evaluation. Inserting $\nu = \mu_1/\mu_2$ into (9b), the characteristic frequency reads

$$\omega_C = \frac{\omega_1 + \omega_2}{2} - \frac{\nu - 1}{\nu + 1}\frac{\omega_1 - \omega_2}{2}.$$

C. Example 3: Tunability of a single MEMS sensor

Finally, consider a single MEMS sensor with the control law (2). This system is governed by

$$\dot{\boldsymbol{x}} = \begin{bmatrix} x_{i,2} \\ -\omega_0^2 x_1 - \frac{\omega_0}{Q_0} x_2 + \alpha x_3 \\ -\beta x_3 + \zeta (k x_4 + u_{DC})^2 \\ -\frac{1}{\tau} x_4 + \kappa x_2 \end{bmatrix},$$
$$t > 0, \quad \boldsymbol{x}(0) = \boldsymbol{x}_0. \tag{10}$$

Note that system (10) has two different Andronov–Hopf bifurcations, which are controlled by the feedback strength k. This is summarized in detail subsequently.

Theorem 1 (Rolf and Meurer[10]). *System (10) undergoes two Andronov–Hopf bifurcations depending on the feedback gain k. The critical points $k_H^{\pm}$ and the characteristic frequencies $\omega_C^{\pm}$ at the critical point are given by*

$$k_H^{\pm} = \frac{2a_1 - a_2 a_3 \pm a_3\sqrt{a_2^2 - 4a_0}}{2b_1},$$
$$\omega_C^{\pm} = \sqrt{\frac{a_2 \pm \sqrt{a_2^2 - 4a_0}}{2}},$$

with the coefficients given by (5).

In particular, the characteristic frequencies are determined by the geometry and the material constants of the sensor so that the characteristic frequency cannot be controlled by the feedback strength k and the DC-voltage u_{DC}. This comes from the fact that the considered system represents a cantilever, e.g., see Example 6.7 in Reedy.[58] Hence, the characteristic frequency of system (10) is not tunable.

D. Focus of the work

Based on the results from the examples, the aim of this work is to investigate, if frequency tunability can be achieved in a network of MEMS sensors by controlling the network's asymmetry. Herein, the asymmetry is adjusted by the effective Q-factor of each MEMS sensor. Particularly, these Q-factors are controlled by the feedback strengths k_{ii} for the oscillators $i = 1, \ldots, N$. This conclusion follows from analyzing the necessary conditions of the Andronov–Hopf bifurcations of the coupled MEMS sensors given by (1), i.e., the eigenvalues of the system matrix A have two complex conjugated eigenvalues on the imaginary axis. It should be noted that the remaining conditions, i.e., the eigenvalue crossing condition and the stability of the limit cycle, are not analyzed in detail. In particular, it is trivial to show that the limit cycle is unstable. This comes from the fact that the nonlinearity in (1) is quadratic so that by employing the center manifold theorem[13,45] and inserting the critical point a center manifold with a quadratic nonlinearity in the neighborhood of the equilibrium arises.

IV. BIFURCATION ANALYSIS OF TWO GROUPS OF MEMS SENSORS

Theoretical results are presented to determine the critical point of an interconnection of two different groups of oscillators. It is assumed that the uncoupled oscillators exhibit at least a single Andronov–Hopf bifurcation in terms of a bifurcation parameter. For instance, (10) satisfies this assumption in terms of the feedback strength k. Based on this, the bifurcations of MEMS sensors in the coupled case are analyzed. It turns out that the necessary conditions for the emergence of an Andronov–Hopf bifurcation of two coupled groups of MEMS sensors are satisfied in three cases. Finally, the three critical points are examined in view of the emergence of a Hopf–Hopf bifurcation. The latter arises if two critical points are identical for a given parameter configuration.[30,45,46]

A. Theoretical results

Before discussing the main results of this paper, the definition of a group of oscillators is given.

Definition 2. *A group is a network of identical oscillators. The coupling inside a group is called self-coupling, the coupling between groups is called cross coupling, and the feedback of each oscillator onto itself is called self-feedback.*

In particular, the adjacency matrix of two coupled groups can be written as a block matrix

$$K = \begin{bmatrix} K_{11} & K_{12} \\ K_{21} & K_{22} \end{bmatrix},$$

with the self-coupling matrices K_{11}, K_{22} and the cross-coupling matrices K_{12}, K_{21}. This decomposition of a network into groups is motivated by the fact that each group can be interpreted as an oscillator with multiple critical points. Thus, with this interpretation, the analysis of identical oscillators might be generalized to divide the oscillators into identical oscillators and then to analyze their dynamical behavior. This is subsequently elaborated for two groups.

To determine the critical points of two coupled groups, the structure of the linearization of (1) is exploited. Note that this structure can be induced in the following way:

Assumption 1. *For a network composed of oscillators, the following assumptions are imposed:*

(A1) *The equilibria of the decoupled oscillators are invariant to coupling, i.e., they remain the sole equilibria of the coupled nonlinear system, and the system matrix is influenced by the adjacency matrix.*

(A2) *For each uncoupled oscillator, there exists a critical value $k_{\mathrm{H},ii}$ of the self-feedback strength so that it undergoes at least one Andronov–Hopf bifurcation.*

As a consequence of (A1), the transfer matrix of the coupled system is obtained by coupling the transfer functions of the uncoupled oscillators. Assumption (A2) implies that the Jacobian A_{ii} has a pair of complex conjugated eigenvalues on the imaginary axis for $k_{ii} = k_{\mathrm{H},ii}$. For instance, the critical feedback strength of a single MEMS sensor is given in Theorem 1. The conditions for the critical point of the two coupled groups of oscillators are elaborated as follows.

Theorem 2. *Consider two groups composed of $N_1 \in \mathbb{N}$ and $N_2 \in \mathbb{N}$ oscillators, respectively, so that the dimension of the coupled network is $N = N_1 + N_2$. Let the transfer function of an individual (linearized) oscillator, the self-coupling matrices, and the cross-coupling matrices be given by $g_i(s) \in \mathbb{C}$, $K_{ii} = k_{ii} I \in \mathbb{R}^{N_i \times N_i}$ with the self-feedback in terms of $k_{ii} \in \mathbb{R}$, and $K_{ij} \in \mathbb{R}^{N_i \times N_j}$ for the groups i, $j = 1, 2$ and $i \neq j$. Assume that the eigenvalues $\lambda_k \in \mathbb{R}$, $k = 1, \ldots, N_2$ of the matrix $K_{21}K_{12} \in \mathbb{R}^{N_2 \times N_2}$ are real-valued and the bifurcation parameters. Then, the bifurcation points λ_{H} of the Andronov–Hopf bifurcations of the two groups of oscillators are determined by*

$$\lambda_{\mathrm{H}} = q_{11}^2 + q_{12}^2 - q_{21}^2 - q_{22}^2, \tag{11}$$

with the constants $q_{11}, q_{12}, q_{21}, q_{22} \in \mathbb{R}$ computed from

$$\begin{aligned} 0 &= g_1(\mathrm{i}\omega_{\mathrm{C}}) - g_2(\mathrm{i}\omega_{\mathrm{C}}) \\ &\quad + [k_{11} - k_{22} + 2(q_{21} - \mathrm{i}q_{12})] g_1(\mathrm{i}\omega_{\mathrm{C}}) g_2(\mathrm{i}\omega_{\mathrm{C}}), \end{aligned} \tag{12a}$$

$$0 = 1 - \left[k_{11} + q_{11} + q_{21} - \mathrm{i}\left(q_{12} + q_{22}\right)\right] g_1(\mathrm{i}\omega_{\mathrm{C}}), \tag{12b}$$

$$0 = q_{11}q_{22} - q_{21}q_{12}, \tag{12c}$$

and $\omega_{\mathrm{C}} \in \mathbb{R}$ the characteristic frequency at the critical point.

Remark 1. *Equation (11) must be interpreted in the sense that at least one eigenvalue λ_k of the matrix $K_{21}K_{12}$ must take the value λ_{H}. Note that this also enables us to deduce information about the topology.*

Proof. To prove the claim, it has to be shown that the transfer matrix of the network has a complex conjugated pair of eigenvalues on the imaginary axis. This is done in three steps: First, the transfer function from output to input of the network is derived depending on the coupling in terms of the adjacency matrix K. Second, the adjacency matrix K is shifted by a diagonal matrix $Q \in \mathbb{C}^{N \times N}$ so that $\tilde{K} = K + Q$ becomes singular. Third, this shift introduces a linear pseudo-feedback into each transfer function. This is then used to show that the transfer function of the network has a complex conjugated pair of eigenvalues on the imaginary axis in terms of the eigenvalues λ_{H} of the matrix $K_{12}K_{21}$. According to (A2), the linearization of the oscillators at their equilibrium yields the transfer functions $g_1(s)$ and $g_2(s)$ given by (4).

Moreover, denote the self-coupling matrix and the cross-coupling matrix of the two groups by $K_{11} = k_{11}I$, $K_{22} = k_{22}I$, K_{12} and K_{21} with the self-feedback in terms of k_{11} and k_{22}. Then, the transfer matrix of the coupled groups from output $\boldsymbol{y} = [y_1 y_2 \cdots y_N]^{\mathrm{T}}$ to input $\Delta\boldsymbol{\nu} = [\Delta\nu_1 \Delta\nu_2 \cdots \Delta\nu_N]^{\mathrm{T}}$ reads

$$H(s) = \begin{bmatrix} \frac{1-k_{11}g_1(s)}{g_1(s)} I_{N_1} & 0 \\ 0 & \frac{1-k_{22}g_2(s)}{g_2(s)} I_{N_2} \end{bmatrix} - \underbrace{\begin{bmatrix} 0 & K_{12} \\ K_{21} & 0 \end{bmatrix}}_{=K_{\mathrm{ND}}}.$$

Notably, by choosing this rather uncommon transfer matrix, the effects of the cross coupling K_{ND} can be investigated directly, since the zeros of $H(s)$ are the poles and, thus, at least a subset of the eigenvalues of the network. Hence, the aim is to show that $H(s)$ has two complex conjugated zeros on the imaginary axis. To express this behavior, assume that there exists an asymmetric shift given by

$$\tilde{K} = K_{\mathrm{ND}} - \underbrace{\begin{bmatrix} (q_1^* + q_2^*) I_{N_1} & 0 \\ 0 & (q_1 - q_2) I_{N_2} \end{bmatrix}}_{=Q}, \tag{13}$$

with the constants $q_1 = q_{11} + \mathrm{i}q_{12} \in \mathbb{C}$ and $q_2 = q_{21} + \mathrm{i}q_{22} \in \mathbb{C}$. Herein, z^* denotes the complex conjugate of a complex number $z \in \mathbb{C}$. To satisfy the necessary condition of an Andronov–Hopf bifurcation, it has to be imposed that $\tilde{K}$ is singular, such that a rank drop argument can be used for the transfer matrix $H(s)$. Following Lemma 2 from Appendix A the determinant of $\tilde{K}$ can be simplified to

$$\det \tilde{K} = \frac{N_1}{N_2} \det\left[\left(q_1^* + q_2^*\right)\left(q_1 - q_2\right) I_{N_2} - K_{21}K_{12}\right].$$

Assuming that at least one eigenvalue of $H(s)$ is not influenced by the cross-coupling matrices implies $\det \tilde{K} = 0$. This is achieved by setting $\left(q_1^* + q_2^*\right)\left(q_1 - q_2\right)$ to the eigenvalues $\lambda_k \in \sigma(K_{21}K_{12})$ of $K_{21}K_{12}$ for all oscillator indices $k = 1, \ldots, N_2$ of group 2. This yields

$$\lambda_k = q_{11}^2 + q_{12}^2 - q_{21}^2 - q_{22}^2 + \mathrm{i}2(q_{12}q_{21} - q_{11}q_{22}),$$

where the imaginary part must vanish since the eigenvalues are assumed to be real-valued. Hence, $q_{11}q_{22} = q_{12}q_{21}$ must be satisfied, which implies (11).

Now, it has to be shown that the transfer matrix $H(s)$ is locally singular for $s \in \{\pm\mathrm{i}\omega_{\mathrm{C}}\}$[59] with the characteristic frequency $\omega_{\mathrm{C}} > 0$. For this, the Jordan decomposition of $\tilde{K} = W^* J W$ is used with the Jordan matrix $J \in \mathbb{R}^{N \times N}$ and a transformation matrix $W \in \mathbb{R}^{N \times N}$.[60] For the output-to-input transfer function of the network, this implies

$$\begin{aligned} H(s) &= \begin{bmatrix} \frac{1-k_{11}g_1(s)}{g_1(s)} I_{N_1} & 0 \\ 0 & \frac{1-k_{22}g_2(s)}{g_2(s)} I_{N_2} \end{bmatrix} - Q - \tilde{K} \\ &= \begin{bmatrix} \frac{1-k_{11}g_1(s)}{g_1(s)} I_{N_1} & 0 \\ 0 & \frac{1-k_{22}g_2(s)}{g_2(s)} I_{N_2} \end{bmatrix} - Q - W^* J W. \end{aligned}$$

By imposing

$$\begin{aligned}&\begin{bmatrix}\frac{1-k_{11}g_1(s)}{g_1(s)}I_{N_1} & 0\\ 0 & \frac{1-k_{22}g_2(s)}{g_2(s)}I_{N_2}\end{bmatrix}-Q\\ &=\begin{bmatrix}\frac{1-(k_{11}+q_1^*+q_2^*)g_1(s)}{g_1(s)}I_{N_1} & 0\\ 0 & \frac{1-(k_{22}+q_1-q_2)g_2(s)}{g_2(s)}I_{N_2}\end{bmatrix}\\ &=h(s)I_N,\quad \forall s\in\{\pm\mathrm{i}\omega_C\},\end{aligned}$$

the transfer matrix is simplified to

$$H(s)=W^*\left(h(s)I-J\right)W,$$

respectively. If $h(s)$ vanishes for $s\in\{\pm\mathrm{i}\omega_C\}$, this implies that $H(s)$ is singular, because J is singular for all $s\in\mathbb{C}$. This analysis implies the following conditions:

$$\begin{aligned}0&=\frac{1-\left[k_{11}+q_1^*+q_2^*\right]g_1(\mathrm{i}\omega_C)}{g_1(\mathrm{i}\omega_C)}\\ &\quad-\frac{1-\left[k_{22}+q_1-q_2\right]g_2(\mathrm{i}\omega_C)}{g_2(\mathrm{i}\omega_C)},\\ 0&=1-[k_{22}+q_{11}-q_{21}+\mathrm{i}(q_{12}-q_{22})]g_2(\mathrm{i}\omega_C),\end{aligned}$$

which can be rearranged into (12a) and (12b), thus concluding the proof. □

Remark 2. *Theorem 2 is also satisfied for two coupled groups of general oscillators if Assumptions (A1) and (A2) are fulfilled and if in addition, no pole-zero cancellation occurs in the elements of the transfer matrix.*

The condition imposed on the real-valued eigenvalues of the product of the cross-coupling matrices $K_{12}K_{21}$ and the self-coupling matrices K_{12} and K_{22} might seem difficult to satisfy. However, this condition is immediately fulfilled, e.g., if

- the network is undirected so that the adjacency matrix becomes symmetric, i.e., $K=K^{\mathrm{T}}$, and
- the size of one group is 1.

Moreover, with a similar argument as in Theorem 2, the bifurcation point of identical oscillators in symmetric networks can be generalized, e.g., see Proposition 1 in Stan and Sepulchre.[15] In particular, the critical point is also shifted by the eigenvalues of the self-coupling matrix in asymmetric networks. This is summarized subsequently.

Proposition 1. *Consider a single group consisting of $N\in\mathbb{N}$ oscillators and denote the self-coupling matrix by $K\in\mathbb{R}^{N\times N}$. In addition, assume that Assumptions (A1) and (A2) are satisfied and that the eigenvalues of the self-coupling matrix $\lambda_i\in\sigma(K)$ are real-valued for the oscillators $i=1,\dots,N$. Then the critical point k_{H} of an Andronov–Hopf bifurcation of each oscillator are given by $k_{\mathrm{H}}=k+\lambda_i$.*

Proof. The proof follows the line of the proof of Theorem 2. However, in the case of one group the auxiliary matrix $Q\in\mathbb{C}^{N\times N}$ simplifies to a weighted identity matrix, i.e., $Q=qI_N$ with the weight $q\in\mathbb{R}$. Then, by following the arguments of the proof of Theorem 2, the conditions

$$\tilde{K}=\det\left[qI_N-K\right],\tag{14}$$

$$G(s)=W^*\left(g(s)I-J\right)W\tag{15}$$

arise. Herein, the parameters are given by the Jordan decomposition $\tilde{K}=W^*JW$ and the transfer function $g(\lambda)\in\mathbb{C}$ of the oscillator. Thus, (14) and (15) have a rank drop, if $q=\lambda_i$ and $k_{\mathrm{H},i}=k+\lambda_i$ for the oscillator $i=1,\dots,N$. The critical point and the feedback strength of the oscillators are then given by $k_{\mathrm{H}}\in\mathbb{R}$ and $k\in\mathbb{R}$, which concludes the proof. □

Remark 3. *By assuming that the oscillators are passive, i.e., the unforced oscillator possesses a stable limit cycle and the feedback system satisfies the dissipation inequality $\dot{S}\le(k-k_{\mathrm{H}})y^2-yh(y)+y\Delta v$ with a nonlinearity $h(y)\in\mathbb{R}$, the critical point of the network becomes unique, i.e., only the minimal eigenvalue changes the critical point. For more details, see Stan and Sepulchre.*[15]

Remark 4. *It has to be stressed that Theorem 2 and Proposition 1 cannot be combined easily. This comes from the fact that the self-coupling matrices are also influencing the complete coupling matrix and its rank. Following the outline of the proof of Theorem 2, rank loss can be induced with an asymmetric shift. This can be analyzed with the determinant*

$$0=\det\left(\begin{bmatrix}K_{11} & K_{12}\\ K_{21} & K_{22}\end{bmatrix}-\begin{bmatrix}(q_1^*+q_2^*)I_{N_1} & 0\\ 0 & (q_1-q_2)I_{N_2}\end{bmatrix}\right).$$

After applying Lemma 1, the determinant can be simplified to

$$\begin{aligned}0&=\det\left(K_{11}-(q_1^*+q_2^*)I_{N_1}\right)\\ &\quad\times\det\left(K_{22}-(q_1-q_2)I_{N_2}\right.\\ &\quad\left.-K_{21}(K_{11}-(q_1^*+q_2^*)I_{N_1})^{-1}K_{12}\right).\end{aligned}\tag{16}$$

Computing the relationship between the critical point and coupling matrix K is, thus, challenging without any further assumptions on (16).

The previous theorem shows that the eigenvalues of the product of the cross-coupling matrices influence the bifurcation behavior. This is simplified by assuming $N_1=N_2$. Then, the bifurcation parameters λ_{H}, which is equal to the critical point, can be decomposed as $\lambda_{\mathrm{H}}=\lambda_{i,\mathrm{H}}^{(12)}\lambda_{j,\mathrm{H}}^{(21)}$. The eigenvalues are given by $\lambda_{i,\mathrm{H}}^{(12)}\in\sigma(K_{\mathrm{H},12})$ and $\lambda_{j,\mathrm{H}}^{(21)}\in\sigma(K_{\mathrm{H},21})$ with the cross-coupling matrices inducing the Andronov–Hopf bifurcation $K_{\mathrm{H},12}\in\mathbb{R}^{N_1\times N_1}$ and $K_{\mathrm{H},21}\in\mathbb{R}^{N_1\times N_1}$ for all oscillator indices $i=1,\dots,N_1$ of group 1 and oscillator indices $j=1,\dots,N_1$ of group 2. This follows directly by considering the eigenvalue problem,

$$K_{\mathrm{H},21}\underbrace{K_{\mathrm{H},12}x}_{=\lambda_{\mathrm{H},12}x}=\lambda_{\mathrm{H},12}\underbrace{K_{\mathrm{H},21}x}_{=\lambda_{\mathrm{H},21}x}=\lambda_{\mathrm{H},12}\lambda_{\mathrm{H},21}x,$$

with the eigenvector $x\in\mathbb{R}^{N_1}$. Hence, the eigenvalues of the adjacency matrices $K_{\mathrm{H},12}$ and $K_{\mathrm{H},21}$ can induce an Andronov–Hopf bifurcation. Interestingly, it also follows that the cross-coupling matrices $K_{\mathrm{H},12}$ and $K_{\mathrm{H},21}$ commute. This observation is generalized to arbitrary networks in the following lemma.

Lemma 1. *The adjacency matrices between the different groups $K_{\mathrm{H},12}$ and $K_{\mathrm{H},21}$ are cumulative for computing the critical point λ_{H}, i.e.,*

$$\sigma(K_{\mathrm{H},21}K_{\mathrm{H},12})\setminus\{0\} = \sigma(K_{\mathrm{H},12}K_{\mathrm{H},21})\setminus\{0\}. \tag{17}$$

Proof. The claim is shown by computing the determinant of a block matrix following Lemma 2 from Appendix A. With this, the determinant of $\tilde{K}$ defined in (13) is given by

$$\det \tilde{K}_{\mathrm{H}} = \tfrac{N_1}{N_2} \det\left[\left(q_1^*+q_2^*\right)\left(q_1-q_2\right) I_{N_2} - K_{\mathrm{H},21}K_{\mathrm{H},12}\right] \tag{18a}$$

$$= \tfrac{N_2}{N_1} \det\left[\left(q_1^*+q_2^*\right)\left(q_1-q_2\right) I_{N_1} - K_{\mathrm{H},12}K_{\mathrm{H},21}\right], \tag{18b}$$

since $q_1^* + q_2^* \neq 0$ and $q_1 - q_2 \neq 0$. This implies (17), which concludes the proof. □

In summary, the bifurcation analysis for a network of two groups of oscillators is simplified by employing Theorem 2 and Lemma 1 in two different ways: First, the conditions of Theorem 2 reduce the degree of the characteristic polynomial. Second, the bifurcation parameter is identified easier, since it is possible to reduce the degree of the characteristic polynomial with Lemma 1 to $\min\{N_1, N_2\}$. Thus, it even might become possible to compute the bifurcation parameter analytically. This is addressed subsequently for two groups motivated by the MEMS-based oscillators (1). In particular, by analyzing the bifurcations of two coupled groups of these oscillators, the characteristic frequency directly follows. Hence, the frequency tunability of two coupled groups can be investigated in this way.

B. Andronov–Hopf bifurcation

After substituting (4) into (12), taking the numerator and splitting it into real and imaginary parts, the resulting equations read

$$0 = [b_{11}b_{21}(k_{11} - k_{22} + 2q_{21}) - a_{21}b_{11} + a_{11}b_{21}]\omega_{\mathrm{C}}^2 + (a_{23}b_{11} - a_{13}b_{21})\omega_{\mathrm{C}}^4, \tag{19a}$$

$$0 = (b_{11} - b_{21})\omega_{\mathrm{C}}^5 + (a_{12}b_{21} - a_{22}b_{11})\omega_{\mathrm{C}}^3 + 2b_{11}b_{21}q_{12}\omega_{\mathrm{C}}^2 + (a_{20}b_{11} - a_{10}b_{21})\omega_{\mathrm{C}}, \tag{19b}$$

$$0 = a_{13}\omega_{\mathrm{C}}^3 + [b_{11}(k_{11} + q_{11} + q_{21}) - a_{11}]\omega_{\mathrm{C}}, \tag{19c}$$

$$0 = \omega_{\mathrm{C}}^4 - a_{12}\omega_{\mathrm{C}}^2 - b_{11}(q_{12} + q_{22})\omega_{\mathrm{C}} + a_{10}, \tag{19d}$$

$$0 = q_{11}q_{22} - q_{21}q_{12}, \tag{19e}$$

with characteristic frequency $\omega_{\mathrm{C}} > 0$ and the constants $q_{ij} \in \mathbb{R}$ for the groups $i, j = 1, 2$. The remaining coefficients are given by (5). In the following, (19) is solved for two different cases: First, the Andronov–Hopf bifurcations of two identical groups with different self-feedback are analyzed. Second, the general case of two non-identical groups consisting of MEMS sensors is discussed.

1. Identical MEMS sensors

In the case of identical groups, (19) is simplified significantly. Furthermore, it is assumed that the feedback strengths k_{11} and k_{22} are different, which yields two groups of oscillators so that Theorem 2 can be applied to obtain

$$0 = b_2^2(k_{11} - k_{22} + 2q_{21})\omega_{\mathrm{C}}^2, \tag{20a}$$

$$0 = 2b_2^2 q_{12}\omega_{\mathrm{C}}^2, \tag{20b}$$

$$0 = a_3\omega_{\mathrm{C}}^3 + (b_2k_{11} + b_2q_{11} + b_2q_{21} - a_1)\omega_{\mathrm{C}}, \tag{20c}$$

$$0 = \omega_{\mathrm{C}}^4 - a_2\omega_{\mathrm{C}}^2 - b_2(q_{12} + q_{22})\omega_{\mathrm{C}} + a_0, \tag{20d}$$

$$0 = q_{11}q_{22} - q_{21}q_{12}. \tag{20e}$$

Solving (20a)–(20d) for q_{11}, q_{12}, q_{21}, and q_{22} results in

$$q_{11} = \frac{a_3\omega_{\mathrm{C}}^2 - a_1}{b_1} + \frac{\tilde{k}_{11} + \tilde{k}_{22}}{2}, \qquad q_{12} = 0,$$

$$q_{21} = -\frac{\tilde{k}_{11} - \tilde{k}_{22}}{2}, \qquad q_{22} = \frac{\omega_{\mathrm{C}}^4 - a_2\omega_{\mathrm{C}}^2 + a_0}{b_1\omega_{\mathrm{C}}},$$

with the shifted self-feedback strengths $\tilde{k}_{ii} = k_{ii} + \lambda_{ii}$ and $\lambda_{ii} \in \sigma(K_{ii})$ for the groups $i = 1, 2$. Substituting this into (20e) and taking the numerator provides

$$0 = \left[2a_3\omega_{\mathrm{C}}^2 - a_1 + b_1(\tilde{k}_{11} + \tilde{k}_{22})\right]\left[\omega_{\mathrm{C}}^4 - a_1\omega_{\mathrm{C}}^2 + a_0\right].$$

It, hence, follows that there are three different parameter configurations satisfying the necessary condition of the Andronov–Hopf bifurcation, i.e.,

$$\lambda_{\mathrm{H}}^{(1)} = \frac{\left(\omega_{\mathrm{C},1}^4 - a_2\omega_{\mathrm{C},1}^2 + a_0\right)^2}{b_1^2\omega_{\mathrm{C},1}^2} - \frac{\left(\tilde{k}_{11} - \tilde{k}_{22}\right)^2}{4}, \qquad \omega_{\mathrm{C},1}^2 = \frac{2a_1 - b_1(\tilde{k}_{11} + \tilde{k}_{22})}{2a_3}, \tag{21a}$$

$$\lambda_{\mathrm{H}}^{(2)} = \frac{a_3\omega_{\mathrm{C},2}^2 - a_1 + b_1\tilde{k}_{11}}{b_1}\frac{a_3\omega_{\mathrm{C},2}^2 - a_1 + b_1\tilde{k}_{22}}{b_1}, \qquad \omega_{\mathrm{C},2}^2 = \frac{a_2 + \sqrt{a_2^2 - 4a_0}}{2}, \tag{21b}$$

$$\lambda_{\mathrm{H}}^{(3)} = \frac{a_3\omega_{\mathrm{C},3}^2 - a_1 + b_1\tilde{k}_{11}}{b_1}\frac{a_3\omega_{\mathrm{C},3}^2 - a_1 + b_1\tilde{k}_{22}}{b_1}, \qquad \omega_{\mathrm{C},3}^2 = \frac{a_2 - \sqrt{a_2^2 - 4a_0}}{2}. \tag{21c}$$

The critical points given by (21b) and (21c) are closely related to the critical points of a single MEMS sensor. This can be seen by imposing $k_{11} = k_{22} = k$. Then, the critical point has to satisfy $\lambda_{\mathrm{H}} = (k_{\mathrm{H}} - k)^2$, where k_{H} is given in Theorem 1. Particularly, this is already predicted by Proposition 1, i.e., the critical point of coupled identical oscillators has to satisfy $k_{\mathrm{H}} = k + \lambda_i$ with the feedback

strength $k \in \mathbb{R}$ and the eigenvalue $\lambda_i \in \sigma(K)$ of the self-coupling matrix K for the oscillators $i = 1, \ldots, N$. However, the additional bifurcation given by (21a) is not predicted as Proposition 1 addresses Andronov–Hopf bifurcations of the uncoupled case. Contrarily, the critical point is given by (21a) is created by coupling the MEMS sensors.

2. Non-identical MEMS sensors

In the case of two non-identical groups of MEMS sensors, (19) has to be solved generally. This is done in the following way: (19a)–(19c) are solved for the constants q_{11}, q_{12}, q_{22}, and the characteristic frequency ω_C. After substituting the results into (19d), a polynomial of third degree arises. Particularly, the emergence of three different critical points can be explained in two different ways. First is by considering the simpler bifurcation behavior of N injectively coupled Andronov–Hopf oscillators. Herein, the eigenvalues of the adjacency matrix are assumed to be the bifurcation parameters. Then, this network has at maximum $N-1$ different Andronov–Hopf bifurcations.[61] For the simplest case, two coupled Andronov–Hopf oscillators have one Andronov–Hopf bifurcation.[25] Second is by considering the results on two coupled groups of identical oscillators, which also have three real-valued critical points.

With these analogies, it follows that a network consisting of two different coupled groups of MEMS sensors has three real-valued bifurcation points, since Theorem 1 implies that one MEMS sensor can described by two Andronov–Hopf oscillators. Thus, it is reasonable to assume that the cubic polynomial has only real solutions.[62] The resulting values for the constants q_{11}, q_{12}, q_{21}, q_{22} and the characteristic frequency ω_C are given in Appendix C.

3. Frequency tunability

In addition to the emergence of the three Andronov–Hopf bifurcations, the three respective characteristic frequencies become tunable by changing the damping of the bifurcation.[25] This is achieved by means of the self-feedback strengths k_{11} and k_{22} as these values in the physical setup change the sensitivity by heating the MEMS sensor, such that the asymmetry in the network can be changed. The limits of the characteristic frequencies can be, e.g., derived by employing first Proposition 1 and then Theorem 2. Proposition 1 implies that the critical points and characteristic frequencies of one group will be given by the individual oscillators if the two groups are not coupled. Thus, if one group is in bifurcation, Theorem 2 implies that there is one critical point equal to zero in the case of two coupled groups. In this case, the characteristic frequency of the two groups is then given by the characteristic frequency of the individual oscillators. In particular, these characteristic frequencies will be the limits for the individual Andronov–Hopf bifurcation, since the characteristic frequency of the system will move toward the characteristic frequency of the other group by increasing the bifurcation parameter of the system. In view of a practical realization, it is desirable that the tunability of the resulting Andronov–Hopf bifurcations is constrained by the neighboring characteristic frequencies so that the closure of the three intervals is empty. This ideal situation is sketched in Fig. 5.

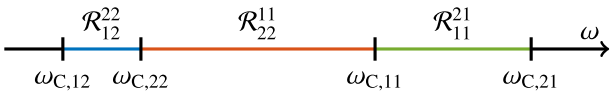

FIG. 5. Sketch of the ideal constraints of the characteristic frequency with the frequency axis ω divided into the optimal intervals $\mathscr{R}_i^j = [\omega_{C,i}, \omega_{C,j}]$ to tune the characteristic frequency for all tuples of group indices $(i,j) \in \{(12,22),(22,11),(11,21)\}$. Herein, $\omega_{C,i}$ denotes a characteristic frequency of one MEMS sensor.

C. Hopf–Hopf bifurcation

Due to the fact that there are three parameter configurations satisfying the necessary condition of an Andronov–Hopf bifurcation the existence of a Hopf–Hopf bifurcation has to be investigated. In general, a Hopf–Hopf bifurcation is a two parameter bifurcation, where the necessary condition for the emergence of a Hopf–Hopf bifurcation is the existence of two purely imaginary, complex conjugated pairs of eigenvalues of the system matrix obtained from the linearization at the equilibrium.[30,45,46] Subsequently, the coupled groups of MEMS sensors are investigated for the emergence of the Hopf–Hopf bifurcation with respect to the frequency difference between the natural frequencies ω_1 and ω_2 and the feedback strength k_{11} and k_{22} for two different scenarios: First, two coupled groups of identical MEMS sensors are investigated. This is done by imposing the additional constraint,

$$\lambda_H^{(i)} = \lambda_H^{(j)}, \tag{22}$$

with the critical points $\lambda_H^{(i)}, \lambda_H^{(j)}$ of the two coupled groups of MEMS sensors for the solutions $i,j = 1,2,3$ and $i \neq j$. In this case, only the feedback strengths k_{11} and k_{22} are discussed. Second, it is argued that it is not possible to derive an analytic equation with (22) for the two coupled non-identical MEMS sensors. Thus, a simple numerical algorithm is shortly proposed to calculate the critical point of a Hopf–Hopf bifurcation for the design parameters.

1. Identical MEMS sensors

Inserting (21a) and (21b) or (21a) and (21c) into (22), results in the quartic equation

$$\begin{aligned} 0 = {} & d_0^{(i)} + d_1^{(i)}(k_{HH,11} + k_{HH,22}) \\ & + d_2^{(i)}(k_{HH,11} + k_{HH,22})^2 - d_3^{(i)}(k_{HH,11} + k_{HH,22})^3 \\ & - b_{11}^4(k_{HH,11} + k_{HH,22})^4, \end{aligned} \tag{23}$$

with the critical feedback strengths $k_{HH,11}$ and $k_{HH,22}$ of the Hopf–Hopf bifurcation. The coefficients are given by

$$\begin{aligned} d_0^{(i)} = {} & -16\left(a_{11} - a_{13}\omega_{C,i}^2\right)\left\{2a_{10}a_{11}a_{13}^2\omega_{C,i}^2 - a_{10}^2a_{13}^3\right. \\ & + \left[a_{13}a_{11}\left(a_{13}^2 - 2a_{12} + \omega_{C,i}^2\right)\right. \\ & \left.\left. + a_{13}^2\left(\omega_{C,i}^4 - (a_{13}^2 + 2a_{12})\omega_{C,i}^2 + a_{12}^2\right) + a_{11}^2\right]a_{11}\omega_{C,i}^2\right\}, \end{aligned}$$

$$d_1^{(i)} = -8b_{11}\left\{a_{13}^3\omega_{C,i}^8 - a_{13}^3\left[a_{13}^2 + 2a_{12}\right]\omega_{C,i}^6 + a_{13}^3\left[a_{12}^2 + 2a_{10} + 4a_{11}a_{13}\right]\omega_{C,i}^4 - a_{11}\left[4a_{11}^2 + 3a_{13}\left(a_{13}^2 - 2a_{12}\right)a_{11} + 2\left(a_{12}^2 + 2a_{10}\right)a_{13}^2\right]\omega_{C,i}^2 + a_{10}^2a_{13}^3\right\},$$

$$d_2^{(i)} = -4b_{11}^2\omega_{C,i}^2\left[a_{13}^2\left(-2a_{13}^2\omega_{C,i}^2 + a_{12}^2 + 2a_{10}\right) + 6a_{11}^2 + \left(3a_{13}^3 - 6a_{12}a_{13}\right)a_{11}\right],$$

$$d_3^{(i)} = 2\left(a_{13}^3 - 2a_{12}a_{13} + 4a_{11}\right)b_{11}^3\omega_{C,i}^2$$

for all the solution indices $i = 2, 3$. This equation can be solved for $k_{HH,11} + k_{HH,22}$ analytically. Note that a similar result can be obtained for the critical points (21a) and (21c). However, a detailed discussion is omitted, since this case follows by replacing $\omega_{C,2}$ with $\omega_{C,3}$.

Consider now the critical points given by (21b) and (21c). These reduce to the same point, if the critical feedback strengths of the Hopf–Hopf bifurcation satisfy

$$k_{HH,11} + k_{HH,22} = \frac{2a_1 - a_2a_3}{b_1}. \tag{24}$$

Moreover, from (23) and (24), it follows that a triple Andronov–Hopf bifurcation, i.e., three purely imaginary pairs of complex conjugated eigenvalues, cannot be obtained by assigning the critical feedback strengths $k_{HH,11}$ and $k_{HH,22}$ since (23) and (24) are linearly dependent.

2. Non-identical MEMS sensors

To derive an analytic equation for the Hopf–Hopf bifurcation, (22) has to be solved for the design parameters, i.e., the feedback strengths k_i or the natural frequency ω_i for the groups $i = 1, 2$. However, this is not possible directly as the resulting equation is transcendental. This comes from the fact that the argument and coefficient of the cosine is given in terms of the second bifurcation parameter. Therefore, the parameters are computed numerically using

$$k_{ii,n+1} = k_{ii,n} + \eta_k\left(\lambda_H^{(j)} - \lambda_H^{(k)}\right), \tag{25a}$$

$$\omega_{i,n+1} = \omega_{i,n} - \eta_\omega\left(\lambda_H^{(j)} - \lambda_H^{(k)}\right), \tag{25b}$$

with the step size $\eta_k, \eta_\omega > 0$ and the iteration $n \in \mathbb{N}$ for the groups $i = 1, 2$ and solutions $j, k = 1, 2, 3$ and $j \neq k$. These iterations are computed individually and are aborted, if the absolute values of the error $e = \lambda_H^{(1)} - \lambda_H^{(3)}$ are smaller than the threshold with respect to the self-feedback $\underline{e}_k > 0$ and the threshold with respect to the natural frequency $\underline{e}_\omega > 0$.

V. SIMULATION RESULTS AND NUMERICAL EVALUATION

Subsequently, the analytical results are verified numerically. First, Theorem 2 is verified for two groups consisting of 6 different MEMS sensors. Herein, it is assumed that $N_1 = 4$ and $N_2 = 2$. Second, the Andronov–Hopf bifurcations are analyzed for an arbitrary topology of the coupled groups. This is done in the following way: First, two coupled, identical groups of MEMS sensors are simulated. Here, the setup is focused on the occurrence of the Hopf–Hopf bifurcation. Afterward, the characteristic frequencies of two coupled non-identical groups of MEMS sensors are investigated. Thereby, it is compared, which pair of eigenvalues passes the imaginary axis first. From now on, this bifurcation will be called dominant since this bifurcation is observed first in the network. Finally, the Hopf–Hopf bifurcation is investigated in terms of the differences between the natural frequencies ω_1 and ω_2 and the feedback strengths k_{11} and k_{22}, respectively.

TABLE I. Parameters of the MEMS sensors.

Parameter		Values
Natural frequency	ω_1	$2\pi \times 3500\ \frac{1}{s}$
	ω_2	$2\pi \times 3750\ \frac{1}{s}$
Q-factor	Q	30,
Offset voltage	u_{DC}	−0.2 V
Transfer factor	α	$19.2\ \frac{m}{Ks}$
Time constant	β	$1006.6\ \frac{1}{s}$
Transfer factor	ζ	4.2588×10^5
Time constant	τ	$10^{-3}\ \frac{1}{s}$
Calibration factor	κ	$10^6\ \frac{V}{m}$
Height	h	1.45×10^{-6} m
Density	ρ	$2,329\ \frac{kg}{m^3}$

Parameters for the MEMS sensors are given in Table I and the parameters for the numerical methods are given in Table II, respectively. It should be noted that the parameters are related to actual MEMS sensors; see, e.g., Lenk *et al.*[9] and Rolf and Meurer.[10] For the assumed parameter set, the two uncoupled MEMS sensors have the possible critical points of the Andronov–Hopf bifurcations $k_{H,11} = 0.109$, $k_{H,12} = -0.296$, $k_{H,21} = 0.163$, and $k_{H,22} = -0.387$. Furthermore, the characteristic frequencies at the critical point are given by $\omega_{C,11} = 2\pi \times 3.505\ \frac{1}{s}$, $\omega_{C,12} = 2\pi \times 159.44\ \frac{1}{s}$, $\omega_{C,21} = 2\pi \times 4.0053\frac{1}{s}$, and $\omega_{C,22} = 2\pi \times 159.47\ \frac{1}{s}$. Note that the equations for the critical point and the characteristic frequency are given in Theorem 1, respectively.

TABLE II. Parameters used in the simulation.

Parameter		Frequency range (Hz)	Values
Step size	η_k	…	10^{-1}
	η_ω	[0, 1 000]	10^6
		[1 000, 7 500]	10^3
		[7 500, 10 000]	10^{-1}
Threshold	$\underline{e}_k$	…	10^{-12}
	$\underline{e}_\omega$	[0, 1 000]	10^{-12}
		[1 000, 7 500]	10^{-9}
		[7 500, 10 000]	10^{-7}
		[10 000, 20 000]	10^{-5}

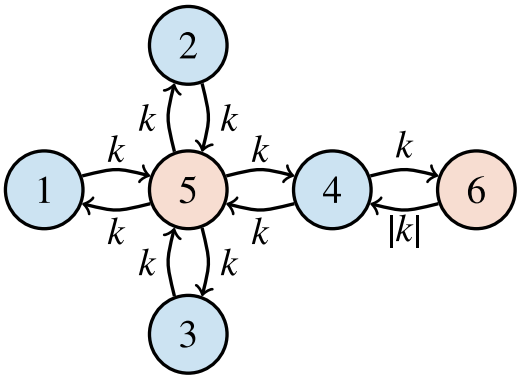

FIG. 6. Sketch of the network topology. Oscillators are colored in terms of their groups.

A. Critical points

In the following, the effects of the network topology on the bifurcations are verified and the location of critical points in terms of the feedback strength is investigated numerically.

1. Critical points of two groups of MEMS sensors

In view of Theorem 2 a network of two groups of MEMS sensors is considered. The topology is shown in Fig. 6. Particularly, the different groups are depicted by the color of the vertex. Thus, the first group consists of $N_1 = 4$ and the second group consists of $N_2 = 2$, respectively. Furthermore, the self-coupling and cross-coupling matrices are given by

$$K_{11} = 0, \qquad K_{12} = \begin{bmatrix} k & k & k & k \\ 0 & 0 & 0 & |k| \end{bmatrix}^{\mathrm{T}},$$

$$K_{21} = \begin{bmatrix} k & k & k & k \\ 0 & 0 & 0 & k \end{bmatrix}, \qquad K_{22} = 0,$$

with the coupling strengths $k \in [-1, 0.5]$. Hence, this network is not symmetric and the product between the cross-coupling matrices is given by

$$K_{21}K_{12} = \begin{bmatrix} 4k^2 & k|k| \\ k^2 & k|k| \end{bmatrix},$$

with the spectrum

$$\sigma(K_{21}K_{12}) = \left\{ \frac{k\left(|k| + 4k \pm \sqrt{16k^2 - 4k|k| + k^2}\right)}{2} \right\}. \tag{26}$$

Starting from $K_{21}K_{12}$, the characteristic polynomial is reduced to a quadratic polynomial so that the critical point can be calculated analytically. Additionally, there are three positive eigenvalues and one negative eigenvalue. In comparison, there are two positive and one negative critical points, resulting in seven different critical points. This observation is illustrated in Fig. 7. Herein, the resulting real part of the minimal eigenvalue of the system matrix in terms of the coupling strength is depicted in Fig. 7(a) and the eigenvalues given by (26) in terms of the parameter $\tilde{k}$ are shown in Fig. 7(b). Particularly, the theoretical results align with numerical simulation, respectively.

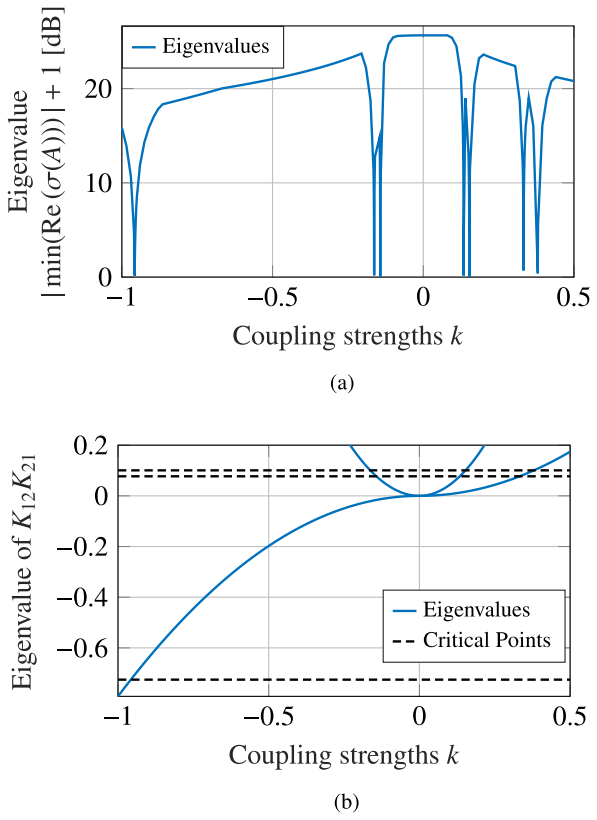

FIG. 7. Comparison between the real part of the minimal eigenvalue of the system matrix A and eigenvalues of matrix $K_{21}K_{12}$ in terms of the coupling strengths $\tilde{k}$. (a) Real part of the minimal eigenvalue of the system matrix A in terms of the coupling strengths $\tilde{k}$. (b) Eigenvalues of the matrix $K_{21}K_{12}$ in terms of the coupling strengths $\tilde{k}$. Herein, the bifurcation points $\lambda_{\mathrm{H}}^{(i)}$, $i = 1, \ldots, 7$ are defined by the intersections of the blue and red curves with the critical points depicted black.

2. Dominant critical point

Subsequently, consider two coupled identical groups of MEMS sensors for the case $k = k_{11} = k_{22}$ with a natural frequency $\omega_1 = 2\pi \times 3500\ \frac{1}{s}$. This system has in total nine possible Hopf–Hopf bifurcations since there are two polynomials of degree 4 and one polynomial of degree 1. The solution of these polynomials is given by

- $k_{\mathrm{HH},1}^{(1,2)} = -0.3$, $k_{\mathrm{HH},2}^{(1,2)} = -0.3$, $k_{\mathrm{HH},3}^{(1,2)} = 0.11$, and $k_{\mathrm{HH},4}^{(1,2)} = 0.11$ between the bifurcations 1 and 2,
- $k_{\mathrm{HH},1}^{(1,3)} = -0.3$, $k_{\mathrm{HH},2}^{(1,3)} = -0.3$, $k_{\mathrm{HH},3}^{(1,3)} = 0.11 + 0.05\mathrm{i}$, and $k_{\mathrm{HH},4}^{(1,3)} = 0.11 - 0.05\mathrm{i}$ between the bifurcations 1 and 3, and
- $k_{\mathrm{HH}}^{(2,3)} = -0.093$ between the bifurcations 2 and 3.

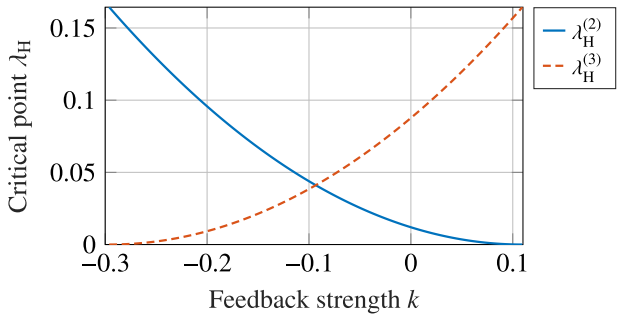

FIG. 8. Critical coupling strength of two coupled, identical, MEMS sensors in terms of a symmetric feedback strength $k(= k_{11} = k_{22})$.

Note that the Hopf–Hopf bifurcation $k_{HH}^{(2,3)}$ is the only valid solution in the sub-critical regime, since it is the only critical point satisfying $k_{H,12} \leq k_{HH}^{(2,3)} \leq k_{H,11}$. Hence, the critical point $k_{HH}^{(2,3)}$ is only investigated further so that the critical coupling strength $\lambda_H^{(1)}$ can be omitted for the analysis, since the critical point $k_{HH}^{(2,3)}$ is not induced by this critical coupling strength. In Fig. 8, the critical point of $\lambda_H^{(2)}$ and $\lambda_H^{(3)}$ in terms of the feedback k is shown. Particularly, by assigning a feedback k, the position of the critical coupling strengths can be changed. For instance, if $k > k_{HH,1}$, then the coupling strength $\lambda_H^{(2)}$ becomes dominant, i.e., $\lambda_H^{(2)}$ is smaller than $\lambda_H^{(3)}$. Hence, it is possible to assign a dominant bifurcation by choosing the feedback strength k, accordingly.

B. Tunability

The tunability of two groups of coupled MEMS sensors is evaluated numerically. This is done by verifying the predictions and investigating the connection between the dominant critical point and the tunability in the sub-critical regime.

1. Characteristic frequency

In the following, the characteristic frequencies $\omega_{C,1}$, $\omega_{C,2}$, and $\omega_{C,3}$ are investigated when the network of two coupled groups is at their corresponding critical points. Furthermore, the variation of the characteristic frequencies in the sub-critical regime is of interest, such that the simulation is performed in terms of the feedback strengths $k_{11} \in [k_{H,12}, k_{H,11}]$ and $k_{22} \in [k_{H,22}, k_{H,21}]$. Moreover, the Hopf–Hopf bifurcation between the first and third Andronov–Hopf bifurcation is computed numerically with (25a), since the numerical values of these two Andronov–Hopf bifurcations have the same sign when choosing appropriate parameters. The variations of the characteristic frequencies $\omega_{C,1}$, $\omega_{C,2}$, and $\omega_{C,3}$ in terms of the feedback strengths k_{11} and k_{22} are shown in Fig. 9. Similar to the two coupled Andronov–Hopf oscillators, the characteristic frequency can be assigned by choosing the feedback strengths k_{11} and k_{22}, accordingly. Interestingly, the simulations lead to the conclusion that the resulting characteristic frequencies can be tuned by controlling the asymmetry of the corresponding network. Moreover, the

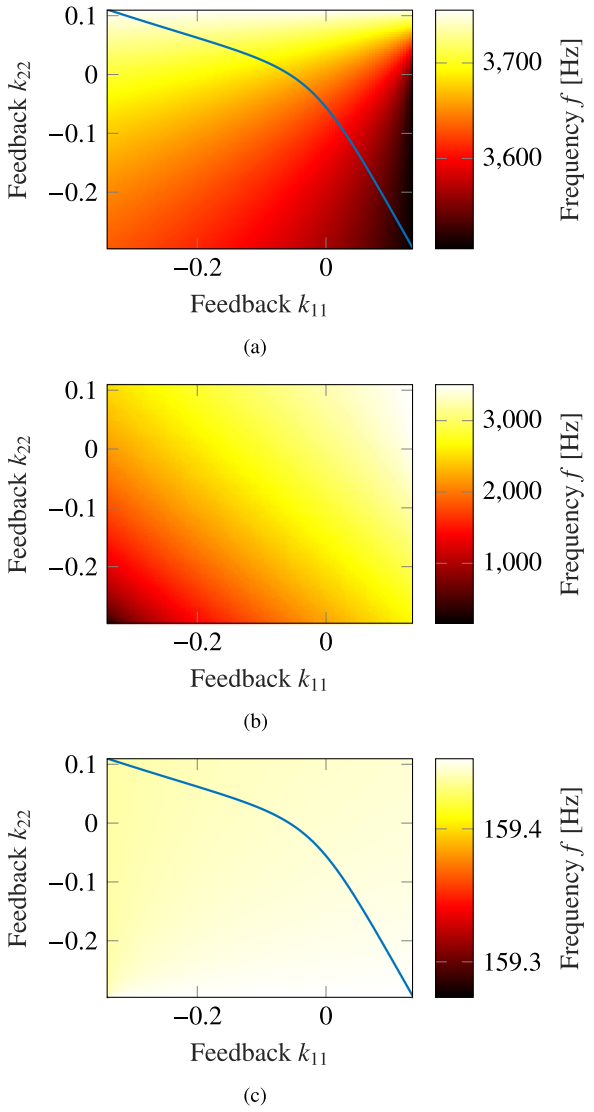

FIG. 9. Characteristic frequency f_C of the three bifurcations in terms of the feedback k_{11} and k_{22}. Herein, the Hopf–Hopf bifurcation between the first and third is visualized by the solid line. (a) Characteristic frequency $f_{C,1}$ in terms of the feedback strengths k_{11} and k_{22}. Herein, the double Andronov–Hopf bifurcation is marked by the blue line. (b) Characteristic frequency $f_{C,2}$ in terms of the feedback strengths k_{11} and k_{22}. (c) Characteristic frequency $f_{C,3}$ in terms of the feedback strengths k_{11} and k_{22}. Herein, the double Andronov–Hopf bifurcation is marked by the blue line.

Hopf–Hopf bifurcation of the bifurcations corresponding to characteristic frequencies $\omega_{C,1}$ and $\omega_{C,3}$ is depicted in Figs. 9(a) and 9(b) by a blue line. Particularly, the regime above the blue line is interesting for a tunable characteristic frequency, since then the bifurcation corresponding to the characteristic frequency $\omega_{C,1}$ is dominant in this regime. Thus, this bifurcation is called tunable from now on. Moreover, this observation leads to the conclusion that the feedback

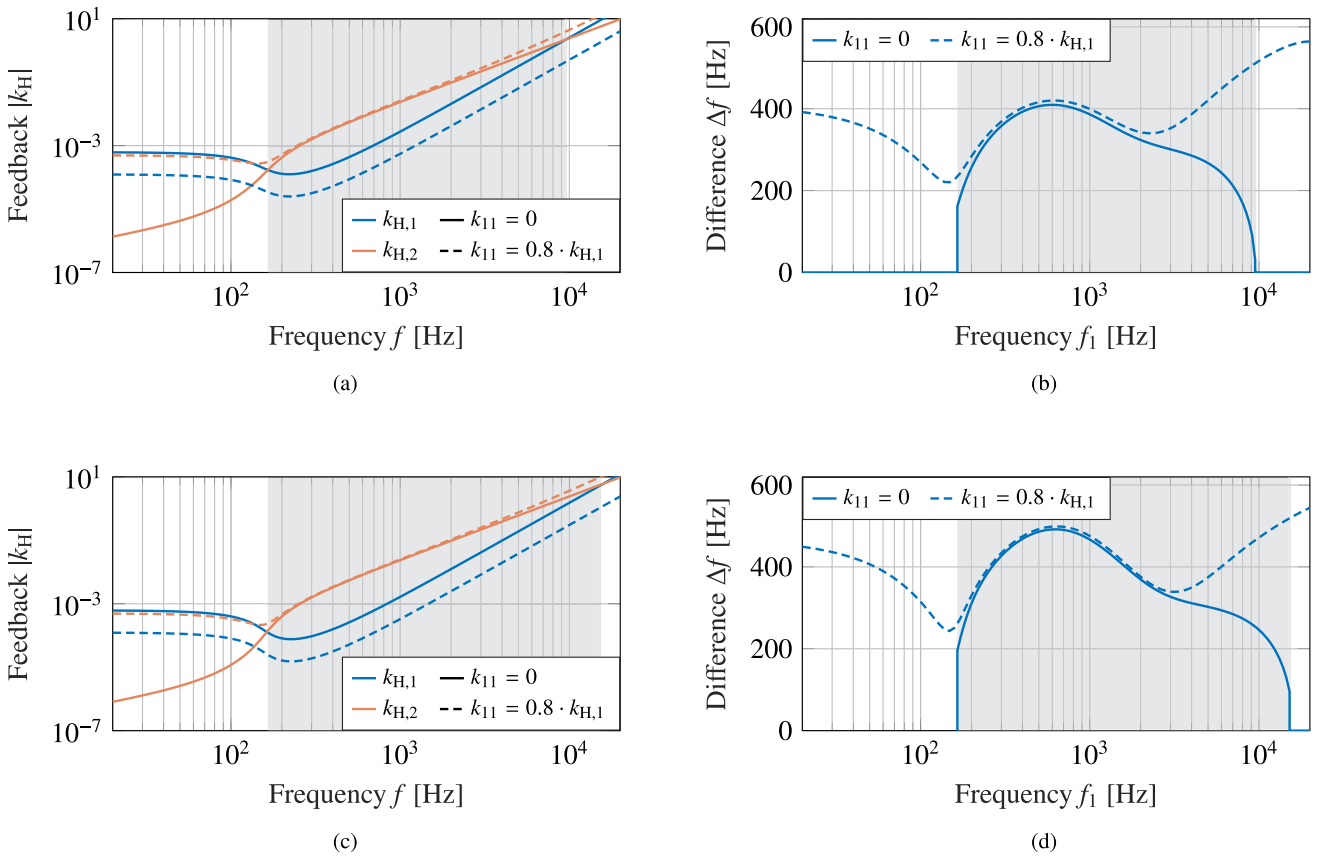

FIG. 10. Comparison between the maximal tunable frequency difference and magnitude of the critical points for different Q-factors. The natural frequency is given by $\omega = 2\pi f$ and the solid lines depict the coupled MEMS sensors without self-coupling, i.e., $k_{11} = 0$. In particular, the tunable interval, i.e., the regime, where the bifurcation becomes dominant, whose characteristic frequency is tunable in the interval $[\omega_1, \omega_2]$, is visualized by the gray area. In contrast to the solid line, the dashed lines show a self-coupling k_{11}, which is shifted toward the critical point $k_{H,1}$, i.e., $k_{11} = 0.8k_{H,1}$. This shift results in a decrease of the magnitude of this critical point so that the tunable frequency difference and its interval is increased. (Top) The Q-factors are given by $Q_1 = Q_2 = 30$. (Bottom) The Q-factors read $Q_1 = Q_2 = 50$. (a) Critical feedback strength k_H of a single MEMS sensor in terms of the natural frequency f. (b) Maximal frequency difference $\Delta f = |f_1 - f_2|$ in terms of the natural frequency f_1. (c) Critical feedback strength k_H of a single MEMS sensor in terms of the natural frequency f. (d) Maximal frequency difference $\Delta f = |f_1 - f_2|$ in terms of the natural frequency f_1.

strengths k_{11} and k_{22} influence, which bifurcation becomes dominant. This comes from the fact that these feedback strengths also influence the eigenvalues, which correspond to the bifurcation.

2. Maximal frequency difference

To evaluate which MEMS sensors can be coupled so that the tunable bifurcation becomes dominant, the maximal difference between the natural frequencies ω_1 and ω_2 of two MEMS sensors is evaluated numerically for different Q-factors, i.e., $Q_i \in \{30, 50\}$ for all $i \in \{1, 2\}$. For this, denote the normalized frequency for a given frequency $\omega > 0$ by $f = \omega/2\pi$. Then, the analysis is done in two steps:

First, the frequency interval $\left[\underline{f}, \bar{f}\right]$ in terms of the feedback strengths k_{11} and k_{22} is investigated. For this, the results obtained for two coupled groups of identical MEMS sensors are used, i.e., the relationship between the critical coupling strengths $k_{H,1}$ and $k_{H,2}$. This is done by evaluating the intersection of the bifurcation points $k_{H,1}$ and $k_{H,2}$ numerically.[63] Second, the frequency difference $\Delta f = |f_1 - f_2|$ is computed with (25b) for the quantified regions numerically. Note that the maximal interval for this investigation is the hearing range of humans, i.e., the interval $\mathscr{R} = [20, 20\,000]$ Hz.[12]

The critical feedback strengths of a single MEMS sensor $k_{H,1}$ and $k_{H,2}$ for the frequency interval $\mathscr{R}$ are depicted in Figs. 10(a) and 10(c) for two different situations. The solid line shows the critical feedback strengths of a MEMS sensor, which is not shifted by feedback. In this situation, the critical feedback strength $k_{H,1}$ is smaller than the other critical feedback strength $k_{H,2}$ in an interval from approximately 165 to 9550 Hz for $Q_i = 30$ and from approximately 165 to 15 170 Hz for $Q_i = 50$, respectively. Note that this interval is marked by the gray region in Fig. 10. In particular, the bifurcation

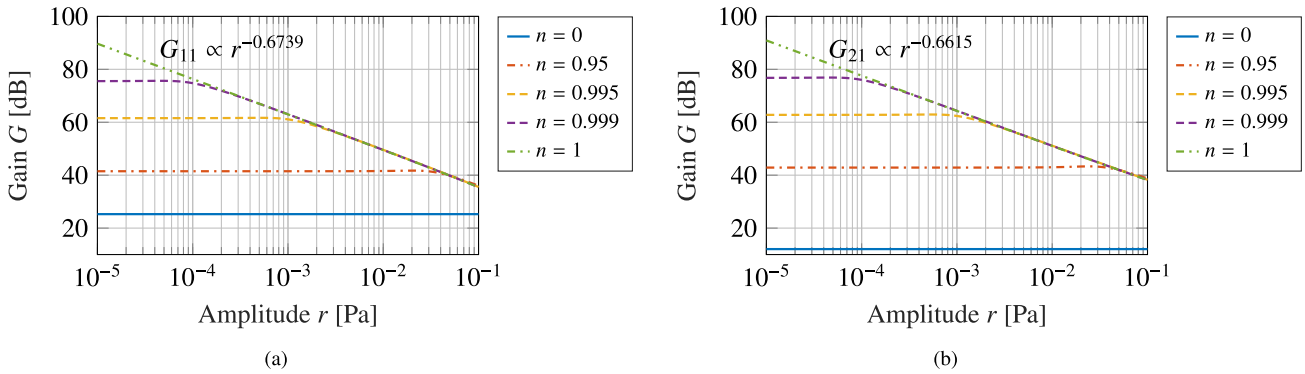

FIG. 11. Gain with respect to the harmonic excitation of the fundamental frequency for the MEMS sensor 1 and MEMS sensor 2 as a function of the amplitude r and the relative coupling strength d. (a) Gain G_{11} of MEMS sensor 1, which can be approximated by $G_{11} \approx 10^{22.434} \times r^{-0.6739}$ V/PA in the nonlinear regime. (b) Gain G_{12} of MEMS sensor 1, which can be approximated by $G_{12} \approx 10^{24.658} \times r^{-0.6615}$ V/PA in the nonlinear regime.

of the characteristic frequency $\omega_{C,1}$ has a smaller magnitude in these intervals rendering it the dominant bifurcation when coupling two identical MEMS sensors. This can be seen from the fact that the critical point of the two coupled identical MEMS sensors is given by the square of the critical feedback strength of a MEMS sensor. For comparison, the network is moved closer to the critical point of the tunable bifurcation. This is done by setting the self-feedback strength critical of one MEMS sensor to $k(\omega) = 0.8 \times k_{H,1}(\omega)$. The results are depicted by the dashed lines. Interestingly, the interval, in which the tunable bifurcation is dominant, is extended to the whole frequency interval $\mathscr{R}$.

With these considerations, the frequency difference Δf is computed numerically. This is done for a system without feedback and a system with feedback relatively close to the critical point of the first MEMS sensor, i.e., $k_{11}(\omega) = 0.8 \times k_{H,1}(\omega)$ and $k_{22} = 0$. The results are shown in Figs. 10(b) and 10(d). In the situation without the shifted feedback, the numerical method converges in an interval from approximately 165 to 9550 Hz for $Q_i = 30$ and from approximately 165 to 15 170 Hz for $Q_i = 50$, respectively. This is depicted by the solid line. Note that in this situation, the dominant bifurcation outside of this interval is given by the characteristic frequency $\omega_{C,3}$. This can be changed by assigning a feedback closer to the critical point $k_{H,1}$ of the first MEMS sensor. Then, the frequency difference has both a larger interval and a larger magnitude. In addition, it can be concluded that an increased Q-factor increased both the intervals, in which the oscillators without shifted feedback, can be coupled.

With the previous simulation, it is shown that the tunability of the characteristic frequencies is achieved in three independent intervals restricted by the characteristic frequencies of the uncoupled MEMS sensors. Herein, the emergence and its respective characteristic frequency of the dominant bifurcation are controlled by the asymmetry of the network, such that the asymmetries can either improve or deteriorate the tunability of two coupled groups. This comes from the fact that the asymmetry between two coupled groups can change their consensus for a limit cycle, such that the tunable critical point might be dominant.

C. Reaction of the system

Finally, the reaction of injectively coupled MEMS sensors is evaluated numerically for different coupling strengths. For practical reasons, only two coupled MEMS sensors are investigated and it is done by employing the so-called envelope mode, which is discussed in Appendix B. In addition, the coupling strength is given as

$$\gamma_{ij} = d\sqrt{\lambda_H^{(k)}},$$

with the relative coupling strength $d \in [0, 1]$ for the oscillators $i, j = 1, 2$, $i \neq j$ and solutions $k = 1, 2, 3$. Herein, the relative gain is assumed to be $d \in \{0, 0.95, 0.995, 0.999, 1\}$ and the fundamental frequency ω_s is asserted to maximize the gain of the system by setting $\omega_s = \omega_C$. The results for the critical Point I are visualized in Fig. 11. The gain G_{11} of MEMS sensor 1 is depicted in Fig. 11(a), while the gain G_{21} of MEMS sensor 2 is shown in Fig. 11(b). It turns out that the gain in the linear regime is different for these sensors. In contrast to this, both MEMS sensors enter the nonlinear regime for the same external amplitude r. To compare the behavior of the MEMS sensors with the cochlea, the compressive nonlinearity of the MEMS sensors is approximated by[64,65]

$$G_{i1} = G_{i0} r^{-p_i}, \tag{27}$$

with the amplitude $r = \sqrt{v_1^2 + v_2^2}$ of the harmonic excitation of the fundamental frequency, the initial gain $G_{i0} > 0$, and the exponent $p_i > 0$ for the oscillators $i = 1, 2$. Fitting (27) for gain G_{11} and G_{21}, results in

$$G_{11} \approx 10^{22.434} \times r^{-0.6739},$$
$$G_{12} \approx 10^{24.658} \times r^{-0.6615}.$$

In comparison, the exponents $p_1 = 0.6739$ and $p_2 = 0.6615$ of the coupled MEMS sensors are similar to the exponent of the cochlea $p_{cochlea} = 2/3$, which has been determined in Dierkes *et al.*[64] and Nadrowski *et al.*.[65]

VI. CONCLUSIONS

The tunability of the resonance frequency of two coupled groups of oscillators undergoing Andronov–Hopf bifurcations is investigated. For this, the respective critical points in the network are derived. Herein, the eigenvalues of the product of the adjacency matrices between these two groups are the bifurcation parameters. In particular, injectively coupled mathematical models of MEMS sensors described by a dominant mode model are considered and the critical points of the arising Andronov–Hopf bifurcations are computed analytically. It turns out that the two coupled groups can exhibit three Andronov–Hopf bifurcations for each eigenvalue of the product between the cross-coupling matrices. In addition, the resonance frequencies of these Andronov–Hopf bifurcations become tunable within physical limits by adjusting the asymmetry of the network. Moreover, the emergence of Hopf–Hopf bifurcations in these networks is studied numerically. This is done by finding a critical feedback strength or a critical natural frequency such that two bifurcation points are equal, such that regions for different consensus are identified. In view of a practical realization, this analysis yields design rules on how two coupled artificial hair cells to achieve high tunability.

ACKNOWLEDGMENTS

This work was funded by the Deutsche Forschungsgemeinschaft (DFG, German Research Foundation)—Project-ID 434434223—SFB 1461. The authors would like to thank Dr. Petro Feketa, Kalpan Ved, and Professor Dr. Claudia Lenk for the enlightening discussions and advice.

AUTHOR DECLARATIONS

Conflict of Interest

The authors have no conflicts to disclose.

Author Contributions

H. F. J. Rolf: Conceptualization (lead); Formal analysis (lead); Software (lead); Visualization (lead); Writing – original draft (lead); Writing – review & editing (equal). **T. Meurer:** Formal analysis (supporting); Funding acquisition (lead); Supervision (supporting); Visualization (supporting); Writing – review & editing (equal).

DATA AVAILABILITY

The data that support the findings of this study are available from the corresponding author upon reasonable request.

APPENDIX A: DETERMINANT OF A BLOCK MATRIX

Lemma A.2 (Ref. 66). *Let* $A \in \mathbb{R}^{N_1\times N_1}$, $B \in \mathbb{R}^{N_2\times N_1}$, $C \in \mathbb{R}^{N_1\times N_2}$, $D \in \mathbb{R}^{N_2\times N_2}$, *A and D invertible, and* $N_1, N_2 \in \mathbb{N}$. *Then, the determinant of the block matrix consisting of A, B, C, and D is given by*

$$\det\begin{bmatrix} A & B \\ C & D \end{bmatrix} = \det(A)\det\left(D - CA^{-1}B\right) = \det(D)\det\left(A - BD^{-1}C\right).$$

APPENDIX B: ENVELOPE MODEL OF INJECTIVELY COUPLED MEMS SENSOR

To compare the behavior of the coupled MEMS sensors and the cochlea, the gain of the system (1) has to be determined. Note that the compression in the nonlinear regime is particularly interesting as this can be compared to experimental values.[64,65] The theoretical values of the compression can be obtained by evaluating the equilibrium of the so-called envelope model,[67–69] which can be determined by writing the state vector $\boldsymbol{x}$ and the external input p as a time-dependent Fourier series,

$$\Delta\boldsymbol{\chi} = q_0 + \sum_{i=1}^{N_q}\left[q_{2i-1}\cos(i\omega_s t) + q_{2i}\sin(i\omega_s t)\right], \tag{B1a}$$

$$p = \nu_0 + \sum_{i=1}^{N_q}\left[\nu_{2i-1}\cos(i\omega_s t) + \nu_{2i}\sin(i\omega_s t)\right]. \tag{B1b}$$

The Fourier coefficients, the fundamental frequency, and the number of the modes are given by $q_j(t) \in \mathbb{R}^4$, $\nu_{l,j}(t) \in \mathbb{R}$, $\omega_s > 0$, and $N_q \in \mathbb{N}$ for the modes $j = 0, 1, \ldots, 2N_q$. Substituting (B1) into (1) and sorting terms results in

$$\frac{\mathrm{d}q}{\mathrm{d}t} = A_q q + B_q \boldsymbol{\nu}_1 + \zeta \boldsymbol{f}_q(q), \tag{B2}$$

with the envelope vectors of the state and input $q = [q_0^{\mathrm{T}}, q_1^{\mathrm{T}}, \ldots, q_{2N_q}^{\mathrm{T}}]^{\mathrm{T}} \in \mathbb{R}^{8N_q+4}$, $\boldsymbol{\nu} = [\nu_0, \nu_1, \ldots, \nu_{2N_q}]^{\mathrm{T}} \in \mathbb{R}^{2N_q+1}$ and the vector-valued nonlinearity $\boldsymbol{f}_q(q) \in \mathbb{R}^{8N_q+4}$. The system matrix and the input matrix are given by

$$A_q = \begin{bmatrix} A & 0 & 0 & \cdots & 0 & 0 \\ 0 & A & -\omega_s & \cdots & 0 & 0 \\ 0 & \omega_s & A & \cdots & 0 & 0 \\ \vdots & \vdots & \vdots & \ddots & \vdots & \vdots \\ 0 & 0 & 0 & \cdots & A & -N_q\omega_s \\ 0 & 0 & 0 & \cdots & N_q\omega_s & A \end{bmatrix} \in \mathbb{R}^{(8N_q+4)\times(8N_q+4)},$$

$$B_q = \begin{bmatrix} b & 0 & 0 & \cdots & 0 & 0 \\ 0 & b & 0 & \cdots & 0 & 0 \\ 0 & 0 & b & \cdots & 0 & 0 \\ \vdots & \vdots & \vdots & \ddots & \vdots & \vdots \\ 0 & 0 & 0 & \cdots & b & 0 \\ 0 & 0 & 0 & \cdots & 0 & b \end{bmatrix} \in \mathbb{R}^{(8N_q+4)\times(2N_q+1)},$$

with the vector $b = [0, 1/(\rho h), 0, 0]^{\mathrm{T}} \in \mathbb{R}^4$. Note that the modes are only coupled by $\boldsymbol{f}_{q,ij}(q) = \Delta\boldsymbol{\chi}_4^2$ for the state $i = 3$ and the modes $j = 0, 1, \ldots, N_q$, while the other entries of the nonlinearity vanish, i.e., $f_{q,ij} = \mathbf{0}$ for the states $i = 1, 2, 4$ and the modes $j = 1, 2, \ldots, N_q$. In particular, the coupling between the modes can be determined by truncating the modes larger than N_q, i.e., $l > N_q$. For instance, the nonlinearity $\boldsymbol{f}_{q,4j}$ for $N_q = 2$ is given by (C3) in Appendix C. With these considerations, the gain with respect to the excitation of the fundamental frequency of the kth output with the oscillator index $k = 1, 2, \ldots, N$ is given by[10]

$$G_{kl} = \frac{1}{r}\sqrt{q_{4k,2l-1}^2 + q_{4k,2l}^2}, \tag{B3}$$

with the amplitude $r = \sqrt{\nu_1^2 + \nu_2^2}$ for the oscillators $k = 1, \ldots, N$ and modes $l = 1, \ldots coSize_q$. It has to be stressed that (B3) has to be computed numerically, since the equilibrium of (B2) is a polynomial with a degree larger than 4.[70–73]

APPENDIX C: CRITICAL POINT OF THE ANDRONOV–HOPF BIFURCATIONS

The equations for the matrix Q and the resonance frequency are summarized. For this, let $i = 1, 2, 3$. Then, the bifurcation point of a network consisting of two different MEMS sensor is given by (C1) and (C2). In addition, the nonlinearity f_q of the envelope model for $N = 2$ is given by (C3).

1. Critical point and resonance frequency

$$\omega_{\mathrm{R}}^2 = \frac{a_{11}b_{21} - a_{21}b_{11} - b_{11}b_{21}(k_{11} - k_{22} + 2q_{21})}{a_{13}b_{21} - a_{23}b_{11}}, \tag{C1a}$$

$$q_{11} = \frac{a_{13}[a_{21} + b_{21}(q_{21} - k_{22})] - a_{23}[a_{11} - b_{11}(k_{11} + q_{21})]}{a_{13}b_{21} - a_{23}b_{11}}, \tag{C1b}$$

$$\begin{aligned} q_{12} = {} & \frac{1}{2b_{11}b_{21}(a_{13}b_{21} - a_{23}b_{11})^{3/2}\sqrt{a_{11}b_{21} - b_{11}[a_{21} + b_{21}(k_{11} - k_{22} + 2q_{21})]}} \\ & \times [a_{21}b_{11}(b_{21}(2a_{11}(b_{11} - b_{21}) + a_{12}(a_{13}b_{21} - a_{23}b_{11}) - 2b_{11}(b_{11} - b_{21})(k_{11} - k_{22} + 2q_{21})) + a_{22}b_{11}(a_{23}b_{11} - a_{13}b_{21})) \\ & + b_{21}(a_{11}(b_{21}(a_{12}(a_{23}b_{11} - a_{13}b_{21}) + 2b_{11}(b_{11} - b_{21})(k_{11} - k_{22} + 2q_{21})) + a_{22}b_{11}(a_{13}b_{21} - a_{23}b_{11})) \\ & + b_{11}(k_{11} - k_{22} + 2q_{21})(b_{21}(a_{12}(a_{13}b_{21} - a_{23}b_{11}) - b_{11}(b_{11} - b_{21})(k_{11} - k_{22} + 2q_{21})) + a_{22}b_{11}(a_{23}b_{11} - a_{13}b_{21})) \\ & + a_{11}^2 b_{21}(b_{21} - b_{11}) + a_{10}(a_{23}b_{11} - a_{13}b_{21})^2) + (b_{21} - b_{11})a_{21}^2 b_{11}^2 - a_{20}b_{11}(a_{23}b_{11} - a_{13}b_{21})^2], \end{aligned} \tag{C1c}$$

$$q_{21} = \frac{c_2}{3c_3} - \frac{2}{3|c_3|}\sqrt{c_2^2 + c_1c_3}\cos\left[\frac{2\pi i}{3} + \frac{1}{3}\arccos\left(\frac{c_3}{|c_3|}\frac{9c_1c_2c_3 - 2c_2^2 - 27c_0c_3^2}{2|c_2^2 + c_1c_3|^{\frac{3}{2}}}\right)\right], \tag{C1d}$$

$$\begin{aligned} q_{22} = {} & \frac{1}{2b_{11}b_{21}(a_{13}b_{21} - a_{23}b_{11})^{3/2}\sqrt{a_{11}b_{21} - b_{11}[a_{21} + b_{21}(k_{11} - k_{22} + 2q_{21})]}} \\ & \times [a_{21}b_{11}(b_{21}(a_{12}(a_{13}b_{21} - a_{23}b_{11}) - 2a_{11}(b_{11} + b_{21}) + 2b_{11}(b_{11} + b_{21})(k_{11} - k_{22} + 2q_{21})) + a_{22}b_{11}(a_{13}b_{21} - a_{23}b_{11})) \\ & + b_{21}(a_{11}(b_{21}(a_{12}(a_{23}b_{11} - a_{13}b_{21}) - 2b_{11}(b_{11} + b_{21})(k_{11} - k_{22} + 2q_{21})) + a_{22}b_{11}(a_{23}b_{11} - a_{13}b_{21})) \\ & + b_{11}(k_{11} - k_{22} + 2q_{21})(b_{21}(a_{12}(a_{13}b_{21} - a_{23}b_{11}) + b_{11}(b_{11} + b_{21})(k_{11} - k_{22} + 2q_{21})) + a_{22}b_{11}(a_{13}b_{21} - a_{23}b_{11})) \\ & + a_{11}^2 b_{21}(b_{11} + b_{21}) + a_{10}(a_{23}b_{11} - a_{13}b_{21})^2) + a_{21}^2(b_{11} + b_{21})b_{11}^2 + a_{20}b_{11}(a_{23}b_{11} - a_{13}b_{21})^2]. \end{aligned} \tag{C1e, C1f}$$

2. Auxiliary constants

$$\begin{aligned} c_0 = {} & (-a_{21}b_{11}(b_{21}(2a_{11}(b_{11} + b_{21}) + a_{12}(a_{23}b_{11} - a_{13}b_{21}) - 2b_{11}(b_{11} + b_{21})(k_{11} - k_{22})) + a_{22}b_{11}(a_{23}b_{11} - a_{13}b_{21})) \\ & + b_{21}(a_{11}(b_{21}(a_{12}(a_{23}b_{11} - a_{13}b_{21}) - 2b_{11}(b_{11} + b_{21})(k_{11} - k_{22})) + a_{22}b_{11}(a_{23}b_{11} - a_{13}b_{21})) \\ & + b_{11}(k_{11} - k_{22})(b_{21}(a_{12}(a_{13}b_{21} - a_{23}b_{11}) + b_{11}(b_{11} + b_{21})(k_{11} - k_{22})) + a_{22}b_{11}(a_{13}b_{21} - a_{23}b_{11})) + a_{11}^2 b_{21}(b_{11} + b_{21}) \\ & + a_{10}(a_{23}b_{11} - a_{13}b_{21})^2) + a_{21}^2(b_{11} + b_{21})b_{11}^2 + a_{20}b_{11}(a_{23}b_{11} - a_{13}b_{21})^2)(a_{23}(b_{11}k_{11} - a_{11}) + a_{13}(a_{21} - b_{21}k_{22})), \end{aligned} \tag{C2a}$$

$$
\begin{aligned}
c_1 = {} & 2b_{11}b_{21}(a_{13}^2 b_{21}(b_{21}(a_{22}b_{11}(k_{11}-2k_{22}) - a_{12}b_{21}k_{22} - a_{11}a_{22} + a_{10}a_{23}) - 2a_{20}a_{23}b_{11} + a_{21}(2a_{22}b_{11} + a_{12}b_{21})) \\
& + a_{13}(-2a_{21}(b_{21}((2b_{11}+b_{21})(a_{11} - b_{11}k_{11}) + b_{11}(3b_{11}+2b_{21})k_{22}) + a_{22}a_{23}b_{11}^2) \\
& + b_{21}(b_{21}(a_{11} - b_{11}k_{11})(a_{11} - 2a_{12}a_{23} - b_{11}k_{11}) + 2k_{22}(b_{21}(2b_{11}+b_{21})(a_{11} - b_{11}k_{11}) + a_{22}a_{23}b_{11}^2) \\
& - 2a_{10}a_{23}^2 b_{11} + b_{11}b_{21}(3b_{11}+2b_{21})k_{22}^2) + a_{21}^2 b_{11}(3b_{11}+2b_{21}) + a_{20}a_{23}^2 b_{11}^2) + a_{23}(a_{11}b_{11}(2b_{21}(a_{12}a_{23} - (2b_{11}+3b_{21})k_{11} \\
& + (b_{11}+2b_{21})k_{22}) + a_{22}a_{23}b_{11} - 2a_{21}(b_{11}+2b_{21})) + b_{11}^2(a_{21}(-a_{12}a_{23} + 2(b_{11}+2b_{21})k_{11} - 2b_{21}k_{22}) \\
& + k_{11}(b_{21}(2b_{11}+3b_{21})k_{11} - a_{23}(a_{22}b_{11} + 2a_{12}b_{21})) + b_{21}k_{22}(a_{12}a_{23} - 2(b_{11}+2b_{21})k_{11}) + a_{21}^2 + a_{10}a_{23}^2 + b_{21}^2 k_{22}^2) \\
& + a_{11}^2 b_{21}(2b_{11}+3b_{21})) + a_{20}a_{13}^3 b_{21}^2),
\end{aligned} \tag{C2b}
$$

$$
\begin{aligned}
c_2 = {} & -4b_{11}^2 b_{21}^2(a_{13}(b_{21}(2a_{11} - a_{12}a_{23} - 2b_{11}k_{11} + (3b_{11}+b_{21})k_{22}) + a_{22}a_{23}b_{11} - a_{21}(3b_{11}+b_{21})) \\
& + a_{23}(b_{11}(-2a_{21} + a_{12}a_{23} - (b_{11}+3b_{21})k_{11} + 2b_{21}k_{22}) + a_{11}(b_{11}+3b_{21})) - a_{22}a_{13}^2 b_{21}),
\end{aligned} \tag{C2c}
$$

$$
c_3 = 8(a_{13}+a_{23})b_{11}^3 b_{21}^3. \tag{C2d}
$$

3. Nonlinearity of the envelope model

$$
f_{q,30} = \frac{1}{2}k_{11}^2\left(q_{41}^2+q_{42}^2+q_{43}^2+q_{44}^2\right) + k_{12}k_{11}\left(q_{41}q_{81}+q_{42}q_{82}+q_{43}q_{83}+q_{44}q_{84}\right) + \frac{1}{2}k_{12}^2\left(q_{81}^2+q_{82}^2+q_{83}^2+q_{84}^2\right), \tag{C3a}
$$

$$
f_{q,31} = k_{11}k_{12}\left(q_{43}q_{81}+q_{44}q_{82}+q_{41}q_{83}+q_{42}q_{84}\right) + k_{11}^2\left(q_{41}q_{43}+q_{42}q_{44}\right) + k_{12}^2\left(q_{81}q_{83}+q_{82}q_{84}\right), \tag{C3b}
$$

$$
f_{q,32} = k_{11}k_{12}\left(q_{44}q_{81}-q_{43}q_{82}-q_{42}q_{83}+q_{41}q_{84}\right) + k_{11}^2\left(q_{41}q_{44}-q_{42}q_{43}\right) + k_{12}^2\left(q_{81}q_{84}-q_{82}q_{83}\right), \tag{C3c}
$$

$$
f_{q,33} = k_{11}k_{12}\left(q_{41}q_{81}-q_{42}q_{82}\right) + \frac{1}{2}k_{12}^2\left(q_{81}^2-q_{82}^2\right) + \frac{1}{2}k_{11}^2\left(q_{41}^2-q_{42}^2\right), \tag{C3d}
$$

$$
f_{q,34} = k_{11}k_{12}\left(q_{42}q_{81}+q_{41}q_{82}\right) + k_{11}^2 q_{41}q_{42} + k_{12}^2 q_{81}q_{82}, \tag{C3e}
$$

$$
f_{q,70} = \frac{1}{2}k_{21}^2\left(q_{41}^2+q_{42}^2+q_{43}^2+q_{44}^2\right) + k_{22}k_{21}\left(q_{41}q_{81}+q_{42}q_{82}+q_{43}q_{83}+q_{44}q_{84}\right) + \frac{1}{2}k_{22}^2\left(q_{81}^2+q_{82}^2+q_{83}^2+q_{84}^2\right), \tag{C3f}
$$

$$
f_{q,71} = k_{21}k_{22}\left(q_{43}q_{81}+q_{44}q_{82}+q_{41}q_{83}+q_{42}q_{84}\right) + k_{21}^2\left(q_{41}q_{43}+q_{42}q_{44}\right) + k_{22}^2\left(q_{81}q_{83}+q_{82}q_{84}\right), \tag{C3g}
$$

$$
f_{q,72} = k_{21}k_{22}\left(q_{44}q_{81}-q_{43}q_{82}-q_{42}q_{83}+q_{41}q_{84}\right) + k_{21}^2\left(q_{41}q_{44}-q_{42}q_{43}\right) + k_{22}^2\left(q_{81}q_{84}-q_{82}q_{83}\right), \tag{C3h}
$$

$$
f_{q,73} = k_{21}k_{22}\left(q_{41}q_{81}-q_{42}q_{82}\right) + \frac{1}{2}k_{21}^2\left(q_{41}^2-q_{42}^2\right) + \frac{1}{2}k_{22}^2\left(q_{81}^2-q_{82}^2\right), \tag{C3i}
$$

$$
f_{q,74} = k_{21}k_{22}\left(q_{42}q_{81}+q_{41}q_{82}\right) + k_{21}^2 q_{41}q_{42} + k_{22}^2 q_{81}q_{82}. \tag{C3j}
$$

REFERENCES

[1] S. A. Zawawi, A. A. Hamzah, B. Y. Majlis, and F. Mohd-Yasin, "A review of MEMS capacitive microphones," Micromachines **11**(5), 484 (2020).
[2] F. Abreu Araujo *et al.*, "Role of non-linear data processing on speech recognition task in the framework of reservoir computing," Sci. Rep. **10**(1), 328 (2020).
[3] J. Abeßer, "A review of deep learning based methods for acoustic scene classification," Appl. Sci. **10**(6), 2020 (2020).
[4] J. Wu, E. Yılmaz, M. Zhang, H. Li, and K. C. Tan, "Deep spiking neural networks for large vocabulary automatic speech recognition," Front. Neurosci. **14**, 199 (2020).
[5] T. Gold and J. Gray, "Hearing. II. The physical basis of the action of the cochlea," Proc. R. Soc. B: Biol. Sci. **135**(881), 492–498 (1948).
[6] T. Gold, R. J. Pumphrey, and J. Gray, "Hearing. I. The cochlea as a frequency analyzer," Proc. R. Soc. B: Biol. Sci. **135**(881), 462–491 (1948).

[7]A. W. Bronkhorst, "The cocktail party phenomenon: A review of research on speech intelligibility in multiple-talker conditions," Acta Acust. Acust. **86**(1), 117–128 (2000).
[8]E. C. Cherry, "Some experiments on the recognition of speech, with one and with two ears," J. Acoust. Soc. Am. **25**(5), 975–979 (1953).
[9]C. Lenk, P. Hövel, K. Ved, S. Durstewitz, T. Meurer, T. Fritsch, A. Männchen, J. Küller, D. Beer, T. Ivanov *et al.*, "Neuromorphic acoustic sensing using an adaptive microelectromechanical cochlea with integrated feedback," Nat. Electron. **9**, 370–380 (2023).
[10]H. F. J. Rolf and T. Meurer, "Amplitude control for an artificial hair cell undergoing an Andronov-Hopf bifurcation," IFAC-PapersOnLine **56**(1), 181–186 (2023).
[11]J. E. Hall and M. E. Hall, *Guyton and Hall Textbook of Medical Physiology e-Book* (Elsevier Health Sciences, 2020).
[12]K. S. Saladin and L. Miller, *Anatomy & Physiology* (WCB, 1998).
[13]J. E. Marsden and M. McCracken, *The Hopf Bifurcation and Its Applications*, Applied Mathematical Sciences Vol. 19 (Springer-Verlag, New York, 1976).
[14]D. G. Aronson, G. B. Ermentrout, and N. Kopell, "Amplitude response of coupled oscillators," Physica D **41**(3), 403–449 (1990).
[15]G.-B. Stan and R. Sepulchre, "Analysis of interconnected oscillators by dissipativity theory," IEEE Trans. Autom. Control **52**(2), 256–270 (2007).
[16]G. Fussmann, S. Ellner, K. Shertzer, and N. Hairston, "Crossing the Hopf bifurcation in a live predator-prey system," Science (New York, NY) **290**, 1358–60 (2000).
[17]J. Guckenheimer, R. Harris-Warrick, J. Peck, and A. Willms, "Bifurcation, bursting, and spike frequency adaptation," J. Comput. Neurosci. **4**, 257–277 (1997).
[18]J. Guckenheimer and J. S. Labouriau, "Bifurcation of the Hodgkin and Huxley equations: A new twist," Bull. Math. Biol. **55**, 937–952 (1993).
[19]E. M. Izhikevich, "Simple model of spiking neurons," IEEE Trans. Neural Netw. **14**(6), 1569–1572 (2003).
[20]F. Gomez, T. Lorimer, and R. Stoop, "Signal-coupled subthreshold Hopf-type systems show a sharpened collective response," Phys. Rev. Lett. **116**(10), 108101 (2016).
[21]R. Van Buskirk and C. Jeffries, "Observation of chaotic dynamics of coupled nonlinear oscillators," Phys. Rev. A **31**(5), 3332–3357 (1985).
[22]S. Camalet, T. Duke, F. Julicher, and J. Prost, "Auditory sensitivity provided by self-tuned critical oscillations of hair cells," Proc. Natl. Acad. Sci. U.S.A. **97**(7), 3183–3188 (2000).
[23]T. A. J. Duke and F. Jülicher, "Critical oscillators as active elements in hearing," in *Active Processes and Otoacoustic Emissions in Hearing*, edited by G. A. Manley, R. R. Fay, and A. N. Popper, Springer Handbook of Auditory Research Vol. 30 (Springer New York, New York, NY, 2007), pp. 63–92.
[24]V. M. Eguíluz, M. Ospeck, Y. Choe, A. J. Hudspeth, and M. O. Magnasco, "Essential nonlinearities in hearing," Phys. Rev. Lett. **84**(22), 5232–5235 (2000).
[25]H. F. J. Rolf and T. Meurer, "Bifurcation analysis of coupled Andronov-Hopf oscillators: A geometric approach," IFAC-PapersOnLine **55**(30), 504–509 (2022).
[26]C. Lenk, L. Seeber, M. Ziegler, P. Hövel, and S. Gutschmidt, "Enabling adaptive and enhanced acoustic sensing using nonlinear dynamics," in *2020 IEEE International Symposium on Circuits and Systems (ISCAS)* (IEEE, 2020), pp. 1–4, ISSN: 2158–1525.
[27]D. Roeser, S. Gutschmidt, T. Sattel, and I. W. Rangelow, "Tip motion—sensor signal relation for a composite SPM/SPL cantilever," J. Microelectromech. Syst. **25**(1), 78–90 (2016).
[28]C. Lenk, A. Ekinci, I. W. Rangelow, and S. Gutschmidt, "Active, artificial hair cells for biomimetic sound detection based on active cantilever technology," in *2018 40th Annual International Conference of the IEEE Engineering in Medicine and Biology Society (EMBC)* (IEEE, 2018), pp. 4488–4491, ISSN: 1558–4615.
[29]K. Ved, C. Lenk, T. Ivanov, P. Hövel, and M. Ziegler, "Bio-inspired, adaptive acoustic sensor: Sensing properties in dependence of feedback parameters," AIP Conf. Proc. **3062**(1), 040011 (2024).
[30]M. Golubitsky and I. Stewart, *The Symmetry Perspective: From Equilibrium to Chaos in Phase Space and Physical Space* (Springer Science & Business Media, 2003), Vol. 200.
[31]J. J. Collins and I. Stewart, "A group-theoretic approach to rings of coupled biological oscillators," Biol. Cybernet. **71**(2), 95–103 (1994).
[32]J. J. Collins and I. N. Stewart, "Coupled nonlinear oscillators and the symmetries of animal gaits," J. Nonlinear Sci. **3**(1), 349–392 (1993).
[33]G. Schöner, W. Y. Jiang, and S. Kelso, "A synergetic theory of quadrupedal gaits and gait transitions," J. Theor. Biol. **142**, 359–91 (1990).
[34]J. Cohen and I. Stewart, *Polymorphism Viewed as Phenotypic Symmetry-Breaking* (University of Warwick, Mathematics Institute, 1999).
[35]T. Elmhirst, "Symmetry-breaking bifurcations of S_N-equivariant vector fields and polymorphism," M.Sc. thesis (Mathematics Institute, University of Warwick, 1998).
[36]I. Stewart, T. Elmhirst, and J. Cohen, "Symmetry-breaking as an origin of species," in *Bifurcation, Symmetry and Patterns* (Springer, 2003), pp. 3–54.
[37]T. L. Vincent and T. L. S. Vincent, "Evolution and control system design. The evolutionary game," IEEE Contr. Syst. **20**(5), 20–35 (2000).
[38]P. Ashwin and J. W. Swift, "The dynamics of n weakly coupled identical oscillators," J. Nonlinear Sci. **2**, 69–108 (1992).
[39]B. Ermentrout, Y. Park, and D. Wilson, "Recent advances in coupled oscillator theory," Philos. Trans. R. Soc. A: Math. Phys. Eng. Sci. **377**(2160), 20190092 (2019).
[40]G. B. Ermentrout and N. Kopell, "Frequency plateaus in a chain of weakly coupled oscillators, I," SIAM J. Math. Anal. **15**(2), 215–237 (1984).
[41]A. Mauroy and I. Mezić, "On the use of Fourier averages to compute the global isochrons of (quasi)periodic dynamics," Chaos **22**(3), 033112 (2012).
[42]Y. Kuramoto, "Rhythms and turbulence in populations of chemical oscillators," Physica A **106**(1–2), 128–143 (1981).
[43]J. C. Neu, "Coupled chemical oscillators," SIAM J. Appl. Math. **37**(2), 307–315 (1979).
[44]F. C. Hoppensteadt and E. M. Izhikevich, *Weakly Connected Neural Networks* (Springer Science & Business Media, 1997), Vol. 126.
[45]J. Guckenheimer and P. Holmes, *Nonlinear Oscillations, Dynamical Systems, and Bifurcations of Vector Fields* (Springer Science & Business Media, 2013), Vol. 42.
[46]Y. A. Kuznetsov, I. A. Kuznetsov, and Y. Kuznetsov, *Elements of Applied Bifurcation Theory* (Springer, 1998), Vol. 112.
[47]H. F. J. Rolf and T. Meurer, "Enabling tunability of a MEMS sensor with a geometric nonlinearity," IFAC-PapersOnLine **58**(5), 66–71 (2024).
[48]R. G. Ayoub, "Paolo Ruffini's contributions to the quintic," Arch. History Exact Sci. **23**(3), 253–277 (1980).
[49]J. Bewersdorff, *Galois Theory for Beginners: A Historical Perspective*, 2nd ed. (American Mathematical Society, Providence, 2021).
[50]Y.-C. Lee, L.-K. Wang, Y.-C. Chuang, H.-C. Hong, and Y. Chiu, "Electrothermal tunable MEMS oscillators for MEMS-based reservoir computing," IEEE Sens. Lett. **8**(7), 1–4 (2024).
[51]K. B. Lee, L. Lin, and Y.-H. Cho, "A frequency-tunable microactuator with a varied comb-width profile," in *17th IEEE International Conference on Micro Electro Mechanical Systems. Maastricht MEMS 2004 Technical Digest* (IEEE, 2004), pp. 257–260.
[52]R. R. A. Syms, "Electrothermal frequency tuning of folded and coupled vibrating micromechanical resonators," J. Microelectromech. Syst. **7**(2), 164–171 (1998).
[53]J. J. Yao and N. C. MacDonald, "A micromachined, single-crystal silicon, tunable resonator," J. Micromech. Microeng. **5**(3), 257–264 (1995).
[54]S. G. Adams, F. Bertsch, and N. C. MacDonald, "Independent tuning of the linear and nonlinear stiffness coefficients of a micromechanical device," in *Proceedings of Ninth International Workshop on Micro Electromechanical Systems* (IEEE, 1996), pp. 32–37.
[55]K. B. Lee and Y.-H. Cho, "A triangular electrostatic comb array for micromechanical resonant frequency tuning," Sensors Actuat. A **70**(1), 112–117 (1998).
[56]H. Ding, L. Fu, Y. Wang, and J. Xie, "Resonant frequency tunable silicon fishbone-shaped MEMS double ended tuning fork," in *2016 IEEE 11th Annual International Conference on Nano/Micro Engineered and Molecular Systems (NEMS)* (IEEE, 2016), pp. 233–236.
[57]S. H. Strogatz, *Nonlinear Dynamics and Chaos with Student Solutions Manual: With Applications to Physics, Biology, Chemistry, and Engineering* (CRC Press, 2018).
[58]J. N. Reddy, *Energy Principles and Variational Methods in Applied Mechanics* (John Wiley & Sons, 2017).

[59] Without loss of generality, it can be assumed that $s = i\omega_C$, since the transfer matrix of the network $H(s)$ is composed of rational functions $g_1(s)$ and $g_2(s)$ with real-valued coefficients so that complex-valued zeros and poles can only occur in complex conjugated pairs. Particularly, this fact is not changed by adding or subtracting the complex-valued matrix Q, since $H(s)$ is not changed by these manipulations.
[60] K. Kuttler, *An Introduction to Linear Algebra* (Brigham Young University, 2010).
[61] This can be seen by imposing that the characteristic polynomial of the coupled Andronov–Hopf oscillators has N Andronov–Hopf bifurcations for a given adjacency matrix. This is not possible to satisfy, since the rank of the adjacency matrix is $N - 1$.
[62] R. W. D. Nickalls, "A new approach to solving the cubic: Cardan's solution revealed," Math. Gazette **77**(480), 354–359 (1993).
[63] Alternatively, the intersection can be calculated analytically by setting the square root of the critical points in Theorem 1 to zeros so that both bifurcations points have the same value resulting in a Hopf-Hopf bifurcation. This results in a biquadratic equation, which can be solved analytically.
[64] K. Dierkes, B. Lindner, and F. Jülicher, "Enhancement of sensitivity gain and frequency tuning by coupling of active hair bundles," Proc. Natl. Acad. Sci. U.S.A. **105**(48), 18669–18674 (2008).
[65] B. Nadrowski, P. Martin, and F. Jülicher, "Active hair-bundle motility harnesses noise to operate near an optimum of mechanosensitivity," Proc. Natl. Acad. Sci. U.S.A. **101**(33), 12195–12200 (2004).
[66] J. R. Silvester, "Determinants of block matrices," Math. Gazette **84**(501), 460–467 (2000).
[67] V. A. Caliskan, O. C. Verghese, and A. M. Stankovic, "Multifrequency averaging of DC/DC converters," IEEE Trans. Power Electron. **14**(1), 124–133 (1999).
[68] M. Egretzberger and A. Kugi, "A dynamical envelope model for vibratory gyroscopes," Microsyst. Technol. **16**(5), 777–786 (2010).
[69] M. Egretzberger, F. Mair, and A. Kugi, "Model-based control concepts for vibratory MEMS gyroscopes," Mechatronics **22**(3), 241–250 (2012).
[70] H. Broer, H. Hanßmann, and F. Wagener, "Normal resonances in a double Hopf bifurcation," Indagat. Math. **32**(1), 33–54 (2021).
[71] A. Kern and R. Stoop, "Essential role of couplings between hearing nonlinearities," Phys. Rev. Lett. **91**(12), 128101 (2003).
[72] W. Nowacki, P. H. Francis, R. B. Hetnarski, and A. L. Florence, "Dynamic problems of thermoelasticity," J. Appl. Mech. **44**(2), 366 (1977).
[73] B. Wen and K. Boahen, "A silicon cochlea with active coupling," IEEE Trans. Biomed. Circuits Syst. **3**(6), 444–455 (2009).